AGU PUBLICATIONS

JGR

Journal of Geophysical Research: Solid Earth

RESEARCH ARTICLE
10.1002/2013JB010738

Key Points:
- Lacustrine turbidites accurately represent subduction earthquakes in Chile
- Turbidite volume correlates with seismic intensity
- Megathrust earthquake recurrence in Chile is spatially variable

Supporting Information:
- Readme
- Table S1
- Figure S1
- Figure S2
- Figure S3

Correspondence to:
J. Moernaut,
jasper.moernaut@uach.cl

Citation:
Moernaut, J., M. V. Daele, K. Heirman, K. Fontijn, M. Strasser, M. Pino, R. Urrutia, and M. De Batist (2014), Lacustrine turbidites as a tool for quantitative earthquake reconstruction: New evidence for a variable rupture mode in south central Chile, *J. Geophys. Res. Solid Earth*, *119*, 1607–1633, doi:10.1002/2013JB010738.

Received 7 OCT 2013
Accepted 24 FEB 2014
Accepted article online 26 FEB 2014
Published online 21 MAR 2014

Lacustrine turbidites as a tool for quantitative earthquake reconstruction: New evidence for a variable rupture mode in south central Chile

Jasper Moernaut[1,3], Maarten Van Daele[2], Katrien Heirman[2], Karen Fontijn[4], Michael Strasser[3], Mario Pino[1], Roberto Urrutia[5], and Marc De Batist[2]

[1]Facultad de Ciencias, Universidad Austral de Chile, Valdivia, Chile, [2]Renard Centre of Marine Geology, Ghent University, Ghent, Belgium, [3]Geological Institute, ETH Zürich, Zürich, Switzerland, [4]Department of Earth Sciences, University of Oxford, Oxford, UK, [5]Centro EULA, Universidad de Concepción, Concepción, Chile

Abstract Understanding the long-term earthquake recurrence pattern at subduction zones requires continuous paleoseismic records with excellent temporal and spatial resolution and stable threshold conditions. South central Chilean lakes are typically characterized by laminated sediments providing a quasi-annual resolution. Our sedimentary data show that lacustrine turbidite sequences accurately reflect the historical record of large interplate earthquakes (among others the 2010 and 1960 events). Furthermore, we found that a turbidite's spatial extent and thickness are a function of the local seismic intensity and can be used for reconstructing paleo-intensities. Consequently, our multilake turbidite record aids in pinpointing magnitudes, rupture locations, and extent of past subduction earthquakes in south central Chile. Comparison of the lacustrine turbidite records with historical reports, a paleotsunami/subsidence record, and a marine megaturbidite record demonstrates that the Valdivia Segment is characterized by a variable rupture mode over the last 900 years including (i) full ruptures (M_w ~9.5: 1960, 1575, 1319 ± 9, 1127 ± 44), (ii) ruptures covering half of the Valdivia Segment (M_w ~9: 1837), and (iii) partial ruptures of much smaller coseismic slip and extent (M_w ~7.5–8: 1737, 1466 ± 4). Also, distant or smaller local earthquakes can leave a specific sedimentary imprint which may resolve subtle differences in seismic intensity values. For instance, the 2010 event at the Maule Segment produced higher seismic intensities toward southeastern localities compared to previous megathrust ruptures of similar size and extent near Concepción.

1. Introduction

The unexpected large magnitude of recent giant earthquakes along subduction zones (i.e., 2004 M_w 9.2 Sumatra-Andaman; 2010 M_w 8.8 Chile; 2011 M_w 9.0 Tohoku-Oki) emphasizes the shortcomings in the current understanding of megathrust earthquakes and their recurrence patterns. To improve our knowledge and develop correct seismic hazard assessments, high-quality paleoseismic records are required which extend the historical evidence far enough back in time to produce statistically relevant earthquake recurrence data and which are able to register the spatial variability in rupture mode generally found at subduction zones [*Satake and Atwater*, 2007]. In these seismically active regions, records of tsunami deposits and coastal subsidence/uplift can provide valuable paleoseismic data but often lack sufficient spatial coverage, temporal span and, in particular, high temporal resolution. In the marine realm, the detection of turbidity currents immediately following large earthquakes [*Heezen and Ewing*, 1952] or the correlation of turbidite beds to reported earthquakes [*Polonia et al.*, 2013] indicates that sedimentary records of such marine resedimentation events can be used as paleoseismological tools. A systematic turbidite-paleoseismological approach was developed at the Cascadia margin [*Goldfinger*, 2011; *Goldfinger et al.*, 2012] and also successfully applied at the Hikurangi Margin [*Pouderoux et al.*, 2012, 2014] and SW Iberian margin [*Gràcia et al.*, 2010; *Masson et al.*, 2011]. These studies include multiple sediment cores in several turbidite depositional areas to provide continuous records of prehistoric megathrust earthquakes over the last 10–18 kyr. In the Cascadia margin, it also allowed reconstructing temporal variability in rupture area and extent and suggested a possible connection between turbidite mass and earthquake magnitude or shaking intensity [*Goldfinger et al.*, 2012, 2013]. In some studies, the presence/absence of turbidites and the variability in turbidite recurrence rates do not reflect the

megathrust earthquake history due to poor characterization of the local complexity of depositional systems and thus inappropriately selected coring sites [e.g., *Blumberg et al.*, 2008]. Hence, a systematic approach—including multiple cores in several well-selected turbidite deposition areas—is indispensable for using turbidites as paleoseismic indicators.

Historically reported earthquakes along the Chilean subduction zone show relatively short recurrence intervals on the order of a century and complex spatial patterns in which adjacent seismic segments can rupture in only a few years apart and can spatially overlap [*Melnick et al.*, 2009]. To resolve such recurrence patterns, paleoseismic records of ultrahigh (annual to decadal) resolution are needed which is often not feasible in the marine realm, even after correcting turbidite ages for marine reservoir effects and basal turbidite erosion. However, this can be partially countered by accurate correlation of key marker beds, which can be used to prove synchronicity of turbidite deposition in different areas [e.g., *Goldfinger et al.*, 2012].

In lakes, sedimentation rates are relatively high (typically ~1 mm/yr) and annual laminations (varves) can be present in which paleoseismic sediment features can be accurately identified and dated. Also, the generally smaller-scale setting allows for detailed understanding of depositional environments and slope-failure processes. Previous studies investigated the sedimentary record of lakes or closed basins to link soft-sediment deformation, subaquatic landslides, and turbidites with historical earthquake records [e.g., *Sims*, 1973; *Chapron et al.*, 1999; *Arnaud et al.*, 2002; *Monecke et al.*, 2004; *Hubert-Ferrari et al.*, 2012]. It has recently also been shown that increased erosion rates in the catchment due to earthquake-induced landslides can leave distinct sedimentary traces, which can be used as paleoseimic proxy [*Howarth et al.*, 2012; *Avşar et al.*, 2014]. Many studies have shown the great potential of using records of sediment deformation and subaquatic landslides as an archive for reconstructing the paleo-earthquake history in different tectonic settings [e.g., *Karlin and Abella*, 1992; *Schnellmann et al.*, 2002; *Migowski et al.*, 2004; *Moernaut et al.*, 2007; *Beck*, 2009; *Waldmann et al.*, 2011; *Smith et al.*, 2013]. Furthermore, simultaneously triggered, sublacustrine landslides in different lakes can be used to constrain epicenter location and magnitude of their causative paleo-earthquakes [*Strasser et al.*, 2006], and mapping the evolution of slope stability at a basin-wide scale can reveal minimum and maximum values for peak ground accelerations during past events [*Strasser et al.*, 2011]. Nevertheless, lacustrine landslide records can give an underrepresentation of earthquake recurrence at subduction zones [*Moernaut et al.*, 2007], as the interseismic period may not be long enough for a sufficient amount of sediment (and thus static load) to accumulate on a potential sliding surface, and to produce translational slope failures. Instead, records of lacustrine turbidites, for instance, in Lake Biwa in Japan [*Inouchi et al.*, 1996], have been used as a proxy for historical earthquakes that resulted in Modified Mercalli Intensities (MMI) of ≥VII at the lake site. However, the lack of spatial coverage and very limited temporal accuracy so far hampered validating the use of lacustrine turbidites as reliable, quantitative, and continuous paleoseismic recorders.

Our study uses multiple turbidite records with a quasi-annual resolution in several Chilean lake basins and correlates them with historical earthquakes and their local seismic intensity. We propose a new methodology to systematically extract paleoseismic intensity information from turbidite stratigraphies. These results, compiled with other paleoseismic records, lead to a better quantification of magnitude, location, and type of paleo-earthquakes and help improving our understanding of the interplate seismic cycle at the south central Chilean subduction zone.

2. Setting

2.1. Seismotectonic Setting and Earthquake History

South central Chile is tectonically dominated by the slightly oblique subduction of the Nazca Plate under the South American Plate (Figure 1), with an estimated convergence rate of about 6.6 cm/yr based on geodetic data [*Angermann et al.*, 1999], or 7.4 cm/yr based on the analysis of seafloor paleomagnetic data [*DeMets et al.*, 2010]. On 27 February 2010, the Maule earthquake (M_w 8.8) ruptured ~500 km of the subduction megathrust between 33.5°S and 38.5°S and probably closed the Concepción-Constitución seismic gap [*Moreno et al.*, 2012]. The southern part of the 2010 Maule rupture (37–38.5°S) also slipped during the 22 May 1960 Valdivia earthquake (Figure 1), the largest instrumentally recorded earthquake so far (M_w 9.5), and during its largest foreshock on 21 May 1960 (M_w 8.1) [*Cifuentes*, 1989]. South of 38.5°S, the 1960 main event, which had a rupture length of about 1000 km, exhibited its maximum coseismic slip of about 40 m [*Moreno et al.*, 2009]. Associated tsunamis of the 2010 and 1960 events were destructive in the near field with average runup

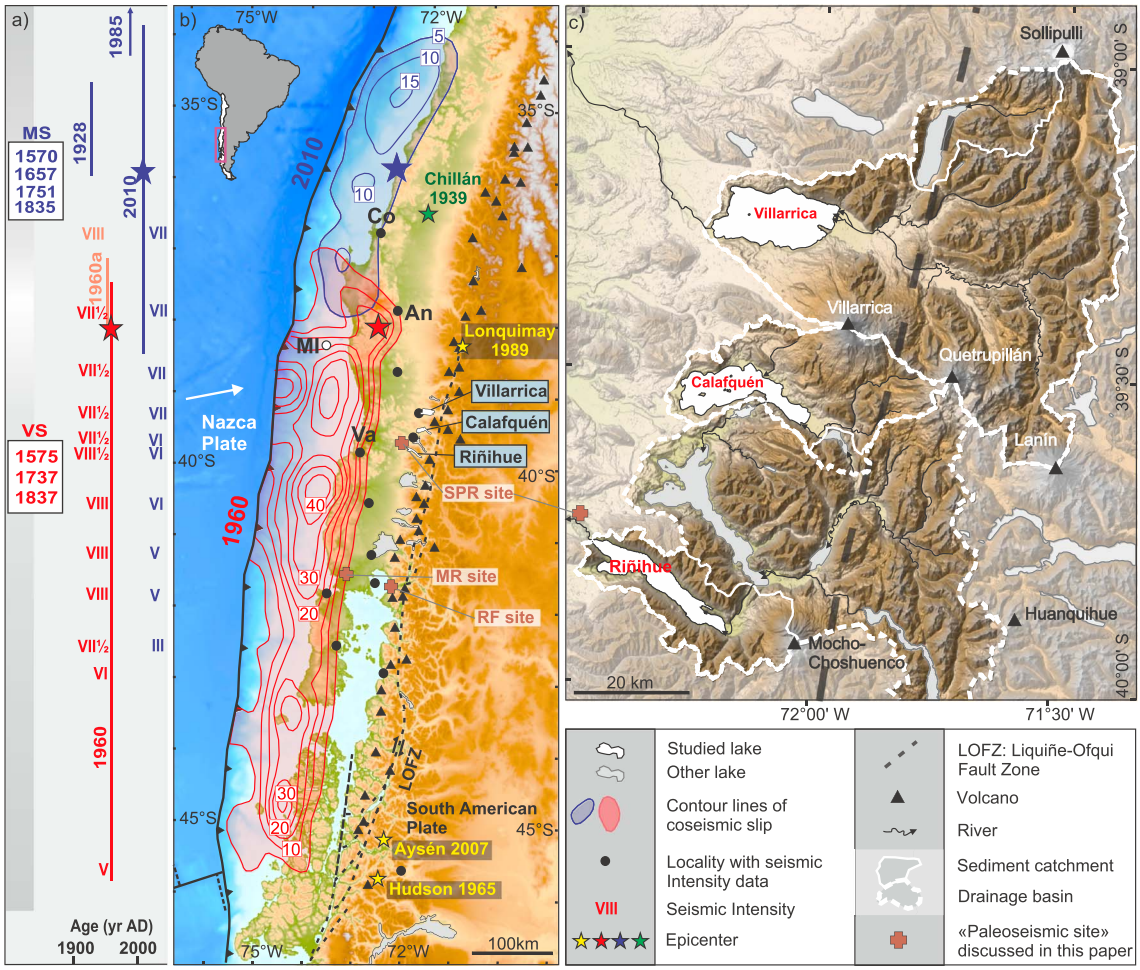

Figure 1. (a) Rupture area of the largest instrumentally recorded megathrust earthquakes in south central Chile. MS: Maule Segment. VS: Valdivia Segment. Roman numerals: seismic intensities for the 2010 [*U.S. Geological Survey*, 2010] and 1960 [*Lazo*, 2008] events at different localities (black dots in Figure 1b). The age of other large historical earthquakes at the MS and VS is shown. (b) Setting of studied lakes at the Andean piedmont and other paleoseismic sites. Red and blue contour lines indicate coseismic slip (isolines every 5 m, starting at 5 m) of the 1960 and 2010 events, respectively [*Moreno et al.*, 2009, 2012]. Epicenter locations of the main earthquakes discussed in the text (interplate (blue and red stars); intraoceanic plate (green stars); crustal (yellow)). Holocene active volcanoes (triangles). LOFZ: Liquiñe-Ofqui Fault Zone [*Melnick et al.*, 2009]. Co: Concepción. Va: Valdivia. An: Angol. SPR: San Pedro River site [*Davis and Karzulovic*, 1963]. MR: Maullín River site [*Cisternas et al.*, 2005]. RF: Reloncaví Fjord site [*St-Onge et al.*, 2012]. (c) Local setting of the studied lakes at the piedmont of the Andes with indication of drainage basins, sedimentary catchments (assuming that lakes are effective sediment traps), and volcanoes. Elevation model based on SRTM data (http://dds.cr.usgs.gov/srtm/).

heights of about 10–15 m [*Sievers*, 2000; *Fritz et al.*, 2011]. Only the 1960 tsunami was destructive in the far field, producing a runup of 10 m in Hawaii and 6 m in Japan [*Cisternas et al.*, 2005].

The 2010 earthquake was the first great megathrust earthquake to be recorded by numerous (31) strong ground motion accelerometers near the rupture zone [*Boroschek et al.*, 2012]. Unfortunately, no instrumental data are available in our study area, the northern part of the Chilean Lake District (39–40°S; Figure 1). Here seismic intensities were obtained from internet-based community questionnaires and averaged around VI–VII on the MMI scale [*U.S. Geological Survey*, 2010]. For the 1960 event, analysis of infrastructural damage in the study area allows inferring a seismic intensity of around VII–VIII on the Medvedev-Sponheuer-Karnik (MSK) scale [*Lazo*, 2008]. In the present study, the mixed usage of these two seismic intensity scales (referred to as "seismic intensity" I) is permitted, as in general, their equivalence is roughly one to one [*Musson et al.*, 2010].

Documented impacts of earthquakes in south central Chile since the arrival of Spanish colonists in 1551 (i.e., "historical" earthquakes) [*Lomnitz*, 1970] delimit two major seismotectonic segments along the subduction megathrust, the Maule Segment (MS) and the Valdivia Segment (VS), matching the 2010 and 1960 rupture areas, respectively [*Métois et al.*, 2012]. Several hypotheses have been put forward to explain

the apparent rupture boundary around 37.5–38.5°S: (i) a marked discontinuity in the continental basement [*Melnick et al.*, 2009], (ii) subducted seafloor relief [*Sparkes et al.*, 2010; *Moreno et al.*, 2011] or large mass-wasting deposits [*Geersen et al.*, 2013] resulting in low interplate coupling, and (iii) splay fault activity accommodating coseismic slip and producing permanent upper plate shortening [*Moreno et al.*, 2012]. In any case, such a tectonic control should result in a persistent seismic segmentation over many interplate earthquake cycles.

At the VS, historical documents revealed a major earthquake and tsunami in 1575 with effects similar to those of the 1960 earthquake [*Cisternas et al.*, 2005]. Also, both events were strong enough to trigger large river-blocking landslides at the San Pedro River (Figure 1), which produced devastating outburst floods [*Davis and Karzulovic*, 1963]. Major earthquakes in 1837 and 1737 also caused severe destruction in the town of Valdivia (40°S), but no large river-blocking landslides and related outburst floods were reported. No tsunami was reported for the 1737 event, whereas the 1837 tsunami was destructive along the southern half of the VS and reached about 6 m high in Hawaii [*Abe*, 1979]. All these suggest that the 1837 and 1737 events probably had a lower magnitude than the 1960 and 1575 events and that the VS may have ruptured only partially. However, historic writings may be spatially deficient (especially in 1737) [*Cisternas et al.*, 2005], so the exact rupture areas are not constrained. Consequently, the role of the 1837 and 1737 events in releasing interseismically accumulated elastic strain at the interplate boundary has not been conclusively established yet.

In Chile, not only the extensive megathrust events but also intraplate earthquakes have been locally destructive. For example, the deadliest earthquake in Chile's history was a tensional intermediate-depth event within the downgoing oceanic slab, i.e., the M_s 7.8 Chillán earthquake in 1939 (Figure 1) [*Beck et al.*, 1998]. Seismic intensity reached about VIII–IX in an area of about 200 km N–S and 120 km E–W. Also, the crustal Liquiñe-Ofqui Fault Zone (LOFZ) within the continental plate is known to have produced three important right-lateral strike-slip earthquakes in modern times (Figure 1) [*Wang et al.*, 2007]: the M_w 6.2 Hudson earthquake in 1965 (45.8°S), the M_s 5.3 Lonquimay earthquake in 1989 (38.5°S), and the M_w 6.2 Aysén earthquake in 2007 (45.2°S). For the 2007 Aysén earthquake, seismic intensities of VII were reported up to a distance of 25 km from its epicenter. Geodetic evidence [*Wang et al.*, 2007] and recent seismicity along the LOFZ [*Lange et al.*, 2008] indicate ongoing seismotectonic activity along this prominent intra-arc shear zone.

2.2. Setting of Studied Lakes and Potential as Earthquake Archive

The studied lakes Villarrica, Calafquén, and Riñihue are located in the northern half of the Valdivia seismotectonic segment between 39°S and 40°S. These glacigenic lakes are relatively large (21 km × 9 km; 24 km × 2-6 km; 28 km × 2–4 km, respectively) and deep (167 m, 212 m, and 323 m, respectively) and are located at the western piedmont of the volcanically active Andes (Figure 1c). Their main inflows are located at their eastern extremities while outflowing rivers originate at their western ends except for lake Calafquén where the outflow is situated in its central eastern part. Since the last deglaciation, a gradual incision of their outflows within the frontal moraines created a generally decreasing trend in lake levels, inversely punctuated by episodes of landslide or volcanic damming of outflows [*Laugenie*, 1982]. In historical times, these open-lake systems have not exhibited large (>5 m) lake-level fluctuations due to their large drainage basins (Figure 1c) and the overall high rainfall regime (~2000 mm/yr) [*Campos*, 1984]. The lakes are oligotrophic and temperate monomictic and exhibit significant seasonal changes in thermal regime, chemical, and biological factors [*Campos*, 1984]. Their bottom morphology is characterized by a central deep basin and shallower areas in the western parts where several sub-basins, bedrock mounds, and moraine ridges are located [*Moernaut*, 2010; *Van Daele et al.*, 2014]. The main inflows deposit the coarsest fraction of their sedimentary load in the associated deltaic fans and in the proximal, deep basins via underflows. An extensive study of sediment cores in lakes Villarrica and Calafquén covering the last ~450 years [*Van Daele et al.*, 2014] shows that the background (i.e., hemipelagic) sedimentation can be classified as a diatomaceous ooze, with a small fraction of terrestrial organic matter, dispersed volcanic ash, and terrigenous clays/silts. It also reveals that lahars, episodically generated syneruptively on the flanks of Villarrica Volcano (Figure 1c), significantly contribute to the sediment budget of the deep proximal basins and can leave thin, fine-grained deposits with a terrestrial composition in the more distal and shallower areas of the lakes. Moreover, thin tephra-fall deposits with distinct geochemical and mineralogical signatures were found throughout the cores, making them useful chronostratigraphic markers for these lake basins. Fine (millimeter-scale) laminations are present in the sedimentary sequences and were deposited annually (i.e., varves), which is attested by radionuclide

dating (^{210}Pb/^{137}Cs) and the nearly one-to-one correlation of volcanic deposits (tephra fall, lahars) to the historical records of volcanic activity [*Van Daele et al.*, 2014]. The annual couplets are composed of a lamina of organic-rich clayey to silty terrestrial material deposited during increased winter river discharge, and a lamina of mainly diatom frustules deposited in spring when diatom blooms occur due to winter nutrient turnover. This depositional cycle has been extensively studied in nearby lake Puyehue (40.7°S) [*Boës and Fagel*, 2008], which has morphological and limnological characteristics similar to those of the three lakes studied here [*Campos*, 1984].

Synchronicity of slope failures in lakes hints at a regional triggering mechanism such as an earthquake [e.g., *Schnellmann et al.*, 2002]. In the southern Andes, this idea was tested by tracing the possible sedimentary fingerprint of the giant 1960 earthquake in several lakes and a fjord [*Chapron et al.*, 2006]. This "synchronicity criterion" was also applied on a seismostratigraphic analysis of landslides in lake Puyehue [*Moernaut et al.*, 2007] and in lake Villarrica [*Moernaut et al.*, 2009]. Lacustrine turbidites were identified in some sediment cores from lakes Villarrica and Calafquén and were tentatively linked to major historical earthquakes in 1960, 1837, 1737 and 1575 [*Van Daele et al.*, 2014]. As the lakes of the present study contain multiple sub-basins, synchronicity of turbidite triggering can be tested within a single lake as well for different lakes.

We focus our study on the distal and shallower sub-basins in the western parts of the lakes (Figure 2) as their depositional regime makes nonseismic triggering of turbidites in those areas rather unlikely. This is due to their morphological protection from hyperpycnal flows originating from the main rivers and from occasional lahars (Figure 2). Also, these isolated sub-basins are out of reach of possible collapses of large deltas which can occur without external triggering mechanism [e.g., *Girardclos et al.*, 2007]. Other types of sedimentary event deposits in our study basins could be created by coastal erosion during large storms [*Meruane et al.*, 2005], subaerial landslides propagating in the lake, runoff events during heavy precipitation or forest fires. However, in all these cases, the sedimentary composition of the associated event deposits would be significantly different (more detrital, terrestrial organic matter, etc.) than for turbidites characterized by remobilization of background sediments (see section 4.2).

3. Methods

The different methodological steps in the analysis of our lacustrine turbidites, eventually leading to the proposition of a variable rupture model, are summarized as a flowchart on Figure 3.

3.1. Reflection-Seismic Data and Sediment Cores

We acquired dense networks of high-resolution reflection-seismic data in lakes Villarrica, Calafquén, and Riñihue (Figures 2a–2c). Two different seismic systems were used: a CENTIPEDE sparker (frequency: 0.4–1.5 kHz) with a single-channel streamer, and a GEOPULSE pinger (frequency: ~3.5 kHz). In the western parts of the lakes, the sparker data allowed imaging the entire sedimentary infill (up to ~100 m) of the lake basins with a vertical resolution of about 37–75 cm. The pinger system penetrated up to ~25 m of the sedimentary fill with a vertical resolution of about 10–20 cm. The deep proximal basins are characterized by limited seismic penetration probably due to biogenic gas in the sediments. After application of a band-pass filter, visualization and seismic-stratigraphic interpretation was done using IHS Kingdom Suite 8.6 [see *Moernaut et al.*, 2009].

Gravity cores (location: Figures 2d–2f) were collected in 2008 and most sites were resampled in 2011 to trace a possible sedimentary imprint of the 2010 Maule earthquake. In order to extract unambiguous and undisturbed paleoseismic records, we selected 25 cores taken in isolated sub-basins in the western parts of the lakes and avoided the proximal deep basins where the volcanic imprints (lahar deposits) are very large or gullies where turbidity currents are erosive [see *Van Daele et al.*, 2014]. Magnetic susceptibility (MagSus) was measured every 2.5 mm on the split core surface with a handheld Bartington MS2E point sensor. We increased the visual contrast and color variability of all core pictures by executing histogram equalization. This image-processing method generates non-natural colors as the most frequent color intensity values on the histogram get most effectively spread. For a selection of cores, scanning electron microscope (JEOL 6400) images of the background sediments were taken and the grain size of untreated sediments was determined using laser diffraction (Malvern Mastersizer 2000) at sampling steps of 0.5 cm.

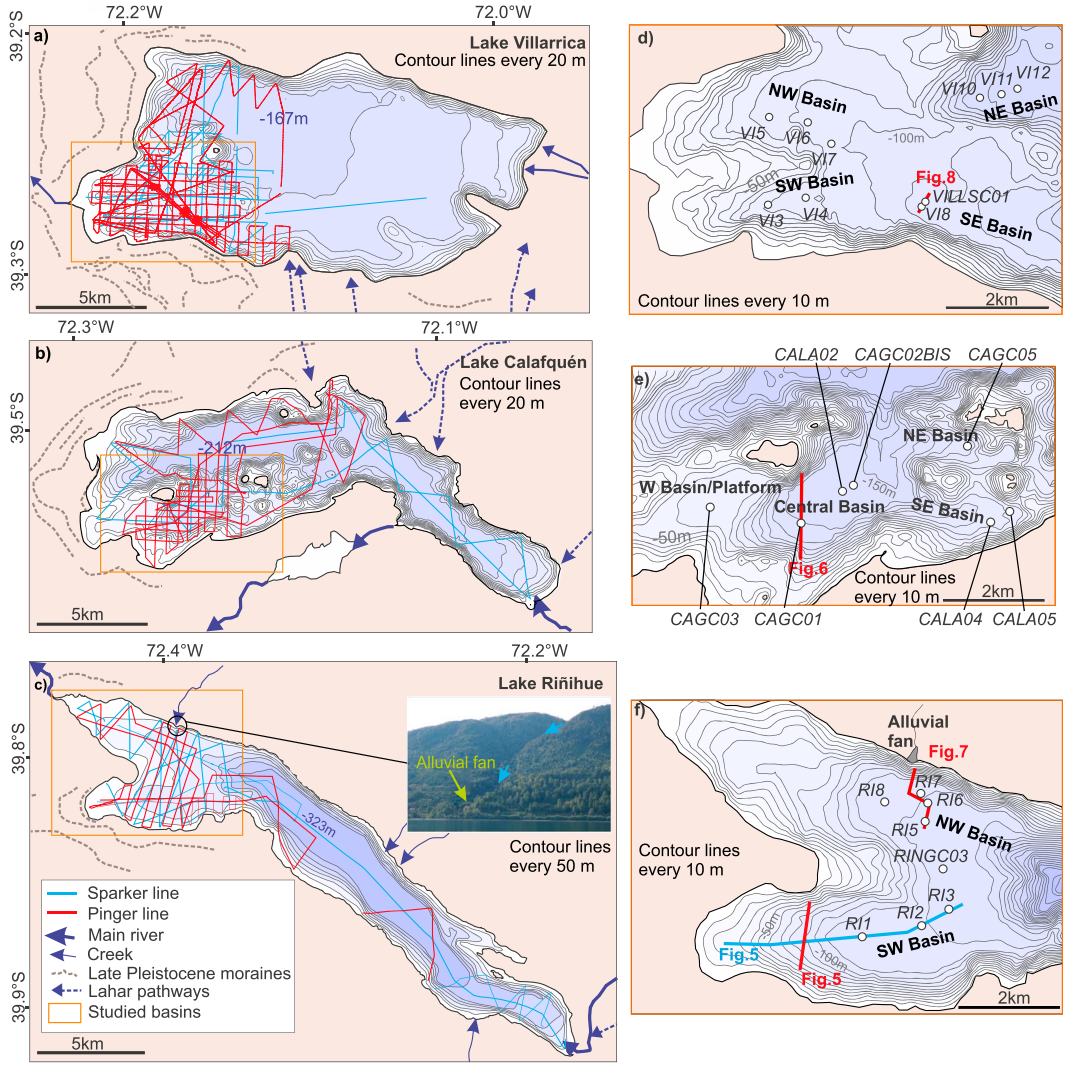

Figure 2. (a–c) Bathymetric maps of the studied lakes with indication of seismic survey lines and main rivers and moraine belts. Bathymetric maps of Villarrica and Calafquén were constructed via interpolation between seismic data and bathymetric data points of the Servicio Hidrográfico y Oceanográfico de la Armada de Chile [*SHOA* (*Servicio Hidrográfico y Oceanográfico de la Armada de Chile*) 1987, 2008]. For lake Riñihue, we used the bathymetric map of *Campos et al.* [1987] for an overview (Figure 2c) and interpolation between seismic profiles for the detailed map (Figure 2f). (inset) Picture of the alluvial fan (discussed in Figure 7) and lake-bordering slopes covered with dense vegetation. (d–f) Detailed bathymetric maps of the studied lake basins with coring sites and seismic profiles presented in this paper.

Lacustrine turbidites were identified in the sediment cores based on their overall homogenous appearance (e.g., Figure 4) in contrast to the finely laminated hemipelagic "background" sedimentation (i.e., diatom ooze with a matrix of volcanic particles, organic matter, and clay). Lacustrine turbidites are characterized by stable or gradually upward decreasing MagSus values as their bottom part can be enriched in coarse clastic material, which has higher MagSus values than diatomaceous ooze [cf. *Bertrand et al.*, 2008]. Discrete chronostratigraphic markers (i.e., tephra-fall and lahar deposits; e.g., Figures 4 and 5) and distinct color changes in the background sediments are used to establish accurate intercore correlations. The glass major element geochemistry and semiquantitative mineral compositions of selected tephra layers in lakes Villarrica and Calafquén were determined using electron microprobe analysis (EMPA; JEOL JXA-8600 Superprobe) and scanning electron microscopy (SEM; JEOL JSM-840A) at the University of Oxford and are presented in *Van Daele et al.* [2014]. Here we add data from lake Riñihue following the same methodology in order to find key stratigraphic marker layers for establishing an interlake correlation framework independent of varve ages.

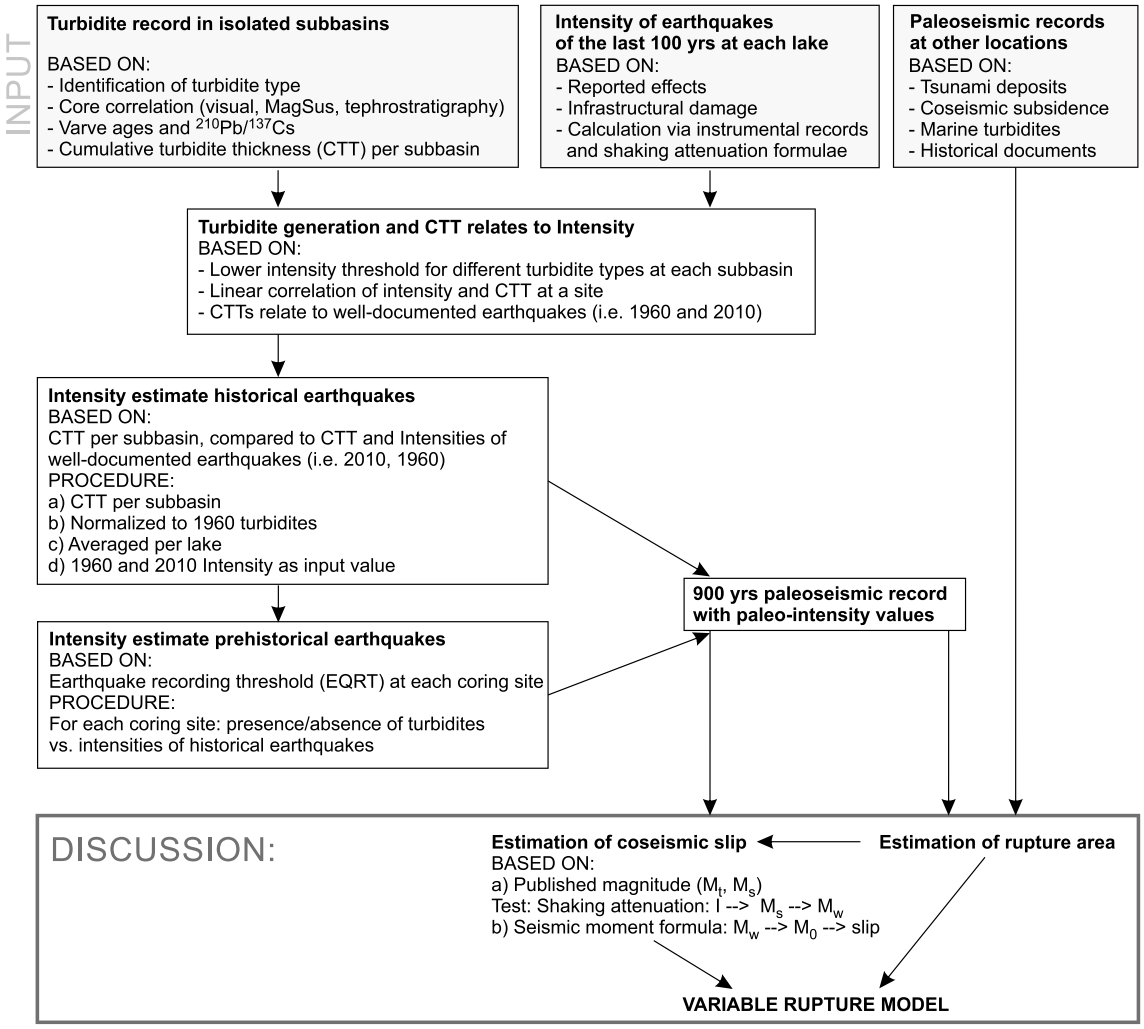

Figure 3. Flowchart illustrating the methodological steps of this study.

Because not enough cores are available to accurately map the complete spatial distribution of turbidites and allow volume calculation, we used the cumulative thickness for each cored turbidite in each sub-basin as an indicator of turbidite volume (CTT: cumulative turbidite thickness). In order to compare between basins and events, we normalized the CTTs to these of the turbidites triggered by the 1960 earthquake. In this way, each studied sub-basin is equally important in the quantification of the overall turbidite stratigraphy, regardless of the amount of cores taken. For interlake comparison, the average value of all sub-basins within each lake is used and can be regarded as a normalized, weighted cumulative turbidite thickness.

3.2. Age-Depth Models

Accurate age-depth models for lakes Villarrica and Calafquén were created by varve counting of impregnated sediment blocks, and a $^{210}Pb/^{137}Cs$ radionuclide profile (Figure S1 in the supporting information) [*Van Daele et al.*, 2014]. Here we apply the same varve-counting procedure on the sediments of lake Riñihue (core RINGC03; see Figure 2f for location). Small errors in the varve age-depth models may be introduced due to preparation disturbance, subjectivity in the counting procedures, and possible erosion below turbidites of maximum a few millimeters [*Van Daele et al.*, 2014]. To minimize errors, we counted each section 3 to 5 times and retained the medium age-depth model. Relative counting errors were estimated as the varve age difference between the medium and outermost models based on different counting sessions for each sediment slab of 10 cm. The relative errors are on average 6%, 5%, and 4% for lakes Villarrica, Calafquén, and Riñihue, respectively. The absolute varve age error of the retained models of Villarrica and Calafquén

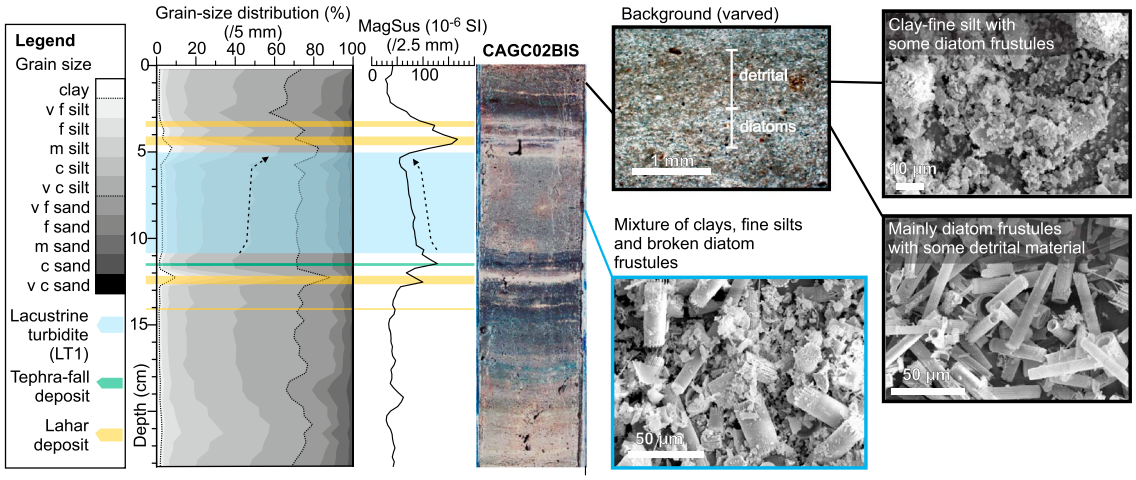

Figure 4. Sedimentological characterization of laminated background sediment and a lacustrine turbidite type 1 (LT1) in core CAGC02BIS (lake Calafquén) using (processed) sediment color, grain-size analysis, magnetic susceptibility, and SEM images. SEM imaging suggests that these LT1s consist of remobilized background sediments. The presented turbidite mainly has a homogenous color, is slightly fining upward, and has a slightly decreasing magnetic susceptibility (MagSus). Specific combinations of MagSus signals and sediment color are also indicative of lahar and tephra deposits [*Van Daele et al.*, 2014].

compared to historically reported eruptions of Villarrica Volcano [*Van Daele et al.*, 2014] culminates around 1600 A.D. to 9 years (2.2 %) and 7 years (1.7 %), respectively, both within the relative error range based on repetitive counting sessions.

A floating chronology model was generated for the estimation of prehistorical turbidite ages in lakes Calafquén and Riñihue. The varve chronologies were anchored to those turbidites which are inferred to have been created by the historical 1575 earthquake (see section 4), and therefore, we report all prehistorical ages in (tuned) varve age A.D. With this tuning, the cumulative age error inherent to varve ages can be drastically reduced. Poor varve quality in cores CALA04 and CALA05 in lake Calafquén made us estimate the age of the oldest turbidite (~1127 ± 44) by extrapolation of the average background sedimentation rate in the period 1321–1575 and exclusion of event deposits. To account for possible slight changes in sedimentation rate (cf. core CAGC02BIS; see section 4.2), we tentatively choose to double the error bar in the extrapolated part.

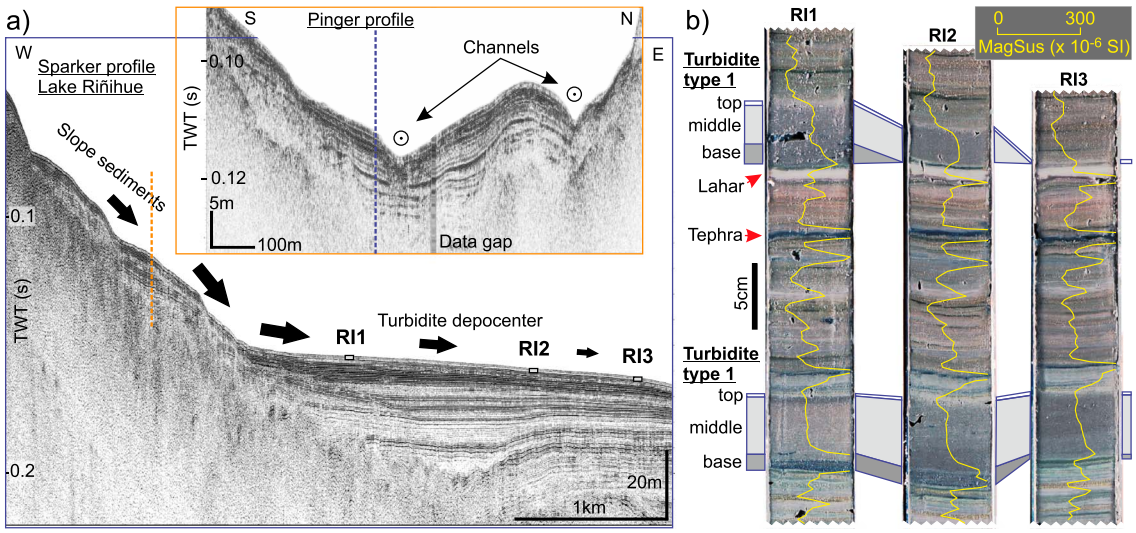

Figure 5. (a) Overview sparker profile in lake Riñihue (location on Figure 2f) illustrating slope sediments and turbidite depocenter. Arrows indicate the direction and volume (not to scale) of sediment transport via turbidity currents (see Figure 5b). (inset) Pinger profile (location: dashed line and Figure 2f) perpendicular to the sparker profile indicating erosive channels in the sedimentary slopes probably confining the turbidity current pathways. (b) Cutout sections of sediment core transect RI1–RI3 showing the downslope evolution of the three main units of turbidites type 1 (LT1). High MagSus and darker color in the turbidites' basal units are indicative of a higher sand content, which is best pronounced in the most proximal core RI1.

Table 1. Seismic Intensity Attenuation Formulae and Formula of Moment Magnitude and Seismic Moment[a]

	Formulae		Reference
	Attenuation		
Interplate (Chile)	$MMI = 1.3844\ M_s - 3.7355\ \mathrm{Log}^{10}(Dr) - 0.0006\ Dr + 3.91$		*Barrientos* [1980]
Intraoceanic plate (Chile)	$MMI = 20.357 - 7.122\ \mathrm{Log}^{10}(Dh) + 0.0017\ Dh$	Santiago 1945 (M_s 7.1)	*Astroza et al.* [2005]
	$MMI = 27.262 - 10.388\ \mathrm{Log}^{10}(Dh) + 0.0056\ Dh$	Punitaqui 1997 (M_s 6.7)	
	$MMI = 28.364 - 10.2\ \mathrm{Log}^{10}(Dh) + 0.0047\ Dh$	La Ligua 1965 (M_s 7.5)	
	$MMI = 29.688 - 10.458\ \mathrm{Log}^{10}(Dh) + 0.0049\ Dh$	Chillán 1939 (M_s 7.8)	
	Moment Magnitude		
	$M_w = 2/3\ (\mathrm{Log}^{10}\ M_o) - 10.7$		*Hanks and Kanamori* [1979]
	Seismic Moment		
	$M_o = \mu\ U\ L\ W$		*Hanks and Kanamori* [1979]

[a]*Dr*: horizontal distance to the closest point of the rupture area. *Dh*: hypocentral distance. *De:* epicentral distance. M_s: surface-wave magnitude. M_w: moment magnitude. M_o: seismic moment. μ: shear modulus of the fault rocks (dyn/cm^2). *L*: length of rupture zone (cm). *W*: width of rupture zone (cm). *U*: average coseismic slip (cm). M_s value for the 1965 La Ligua event according to *Malgrange et al.* [1981]. For intraoceanic plate events, a general attenuation formula that includes magnitude is lacking, so we used the specific attenuation formulae from four studied Chilean earthquakes. We used the formula for the earthquake which has a magnitude equivalent to the considered earthquake, or used the average value between two attenuation formulae of earthquakes with the closest higher and lower magnitude.

3.3. Seismic Intensity Estimation

To evaluate if lacustrine turbidites can be used for quantification of paleoseismic events, we compiled information about the seismic intensity at each lake site for every significant earthquake ($M \geq 7$) during the last 100 years near the study region (section 5; Figure S1 and Table S1). Seismic intensity values were systematically acquired using the MMI scale for the earthquakes of 2011 and 2010 [*U.S. Geological Survey*, 2010; *U.S. Geological Survey,* 2011], and using the MSK scale for the 1960 events [*Lazo*, 2008]. For the other events, we applied empirically derived seismic intensity attenuation formulae (Table 1) accounting for magnitude and the distance of the lake to the earthquake epicenter, hypocenter, or rupture area, for intraoceanic plate and interplate earthquakes, respectively. Earthquake parameters (magnitudes, hypocenter locations, and type of earthquakes) were derived from instrumental data of the *U.S. Geological Survey* [2010, 2011], from scientific literature for the 1960 [*Cifuentes*, 1989] and 1939 events [*Campos et al.*, 2002], and from the SISRA instrumental earthquake data catalogue of South America [*SISRA*, 1985]. Where information about the earthquake type was not available, the earthquake type and parameters were estimated by comparing the hypocenter location and local depth of the interplate boundary derived from *Tassara et al.* [2006]. When the hypocentral depth was not known, seismic intensity values for both interplate and intraoceanic fault sources were calculated using an estimated depth value based on the local depth of the interplate boundary. As the rupture areas of the interplate earthquakes with magnitudes 7.3 or below in our study area (Table S1) are not constrained, we used the epicenter location in the calculations. This may cause only a slight underestimation of seismic intensity (estimated at 0.1–0.3) as earthquakes of magnitudes ≤7.3 are generally not associated with rupture lengths and widths larger than ~70 km and ~45 km, respectively [*Papazachos et al.*, 2004]. For the larger interplate earthquakes (2010, 1960), intensities were acquired by field studies and reports [*Lazo*, 2008; *U.S. Geological Survey,* 2010]. In the present study, the term "seismic intensity" is used in a general way and represents the strength of seismic shaking. It does not directly correlate to the effects of an earthquake on infrastructures, humans, or landscapes in the way seismic scales are classically used. We used one-fourth fractions of an intensity degree to account for spatial variability of shaking strength and for a more accurate calibration to our sedimentary records.

The attenuation formulae show that, for a given magnitude, interplate earthquakes in Chile show lower intensities above the rupture area and lower attenuation gradients than the intraplate events in the oceanic slab [*Saragoni et al.*, 2004]. For extensive interplate ruptures in Chile, seismic ground shaking radiates from multiple asperities along the fault rupture. This means that M_w values, which are dependent on rupture length, do not correlate well with earthquake shaking strength at a given locality, and therefore, M_s values are preferred in the attenuation equations for seismic intensities of large interplate earthquakes.

The calculated intensities need to be treated as an approximate estimate due to error propagation through the instrumental earthquake data, assumptions in the model, and the empirically derived attenuation formulae. This is especially the case for the listed earthquakes in the early twentieth century (e.g., 1920, 1934), the

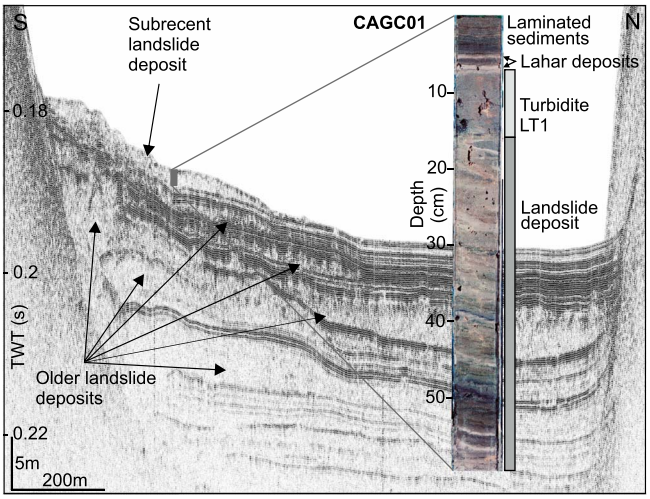

Figure 6. Pinger profile and sediment core (location on Figure 2e) showing a subrecent landslide deposit and associated turbidite (LT1) in the SW sub-basin of lake Calafquén. The landslide deposit consists of a mixture of folded and faulted blocks of laminated sediments and is directly covered (no background sediment in between) by an LT1. Older landslide deposits are present in the seismic stratigraphy at deeper levels.

hypocenter location of which contains probable horizontal and vertical errors of 50–100 km and 40–60 km, respectively [*SISRA*, 1985].

3.4. Back-Calculation of Magnitude and Coseismic Slip

In section 6.5, a rupture model is proposed based on the compilation of our turbidite records, historical, and published paleoseismic data. To test this model, the magnitude and average coseismic slip values of preinstrumental historical earthquakes were calculated. The attenuation formula for Chilean interplate earthquakes (Table 1) [*Barrientos*, 1980] was used to back-calculate the M_s values via the local seismic intensity based on the lacustrine records and the proposed location of the rupture area. Published tsunami magnitude (M_t) or surface wave magnitude (M_s) was converted into moment magnitude (M_w). For the magnitude values considered, M_t approximately equals M_w [*Abe*, 1979], while equivalence to M_s is only valid for M_w lower than 8, as larger M_w values saturate the M_s scale [*Kanamori*, 1983]. Average coseismic slip was then estimated by applying the standard formulae of moment magnitude and seismic moment (Table 1) [*Hanks and Kanamori*, 1979]. We used a shear modulus (μ) of 6.0×10^{10} n/m^2 [*Cifuentes*, 1989], and a rupture width (W) of 140 km as estimated for the 1960 event [*Cifuentes*, 1989], which approximately fits to the width of the thermally defined seismogenic zone [*Völker et al.*, 2011]. Possibly, the studied interplate earthquakes could have ruptured only a part of the seismogenic zone width, and hence, the back-calculated coseismic slip values may be an underestimation.

4. Turbidite Stratigraphy

4.1. Turbidites

In all studied sub-basins, 54 turbidite deposits with thicknesses between 0.5 cm and 7 cm are identified within the sedimentary sequences, based on their macroscopic appearance and MagSus signature (see section 3.1). We discriminate two types of lacustrine turbidites: i.e., lacustrine turbidite type 1 (LT1) and lacustrine turbidite type 2 (LT2) [cf. *Van Daele et al.*, 2014].

A complete sequence of an LT1 is characterized by a thin sandy base, a thick homogenous silty middle unit, and a thin clayey top (Figures 4 and 5). The main middle unit of an LT1 has a similar sedimentary composition and mean grain size than the background sediments. The sandy base and clayey tops both consist of more detrital grains. The LT1s are deposited in basins at the foot of sedimentary slope sequences and are often associated with (i.e., immediately overlying) sublacustrine landslide deposits which were identified on seismic profiles (Figure S2) [e.g., *Moernaut et al.*, 2009] and in sediment cores (Figure 6). Based on these characteristics, as well as on the fact that the isolated basins have no major river input, the respective turbidity currents must have originated from failure of the sediment-covered sublacustrine slopes. In some areas, some shallow coastal material is also entrained in the turbidity currents which results in a slight enrichment of sandy grains and higher MagSus values throughout the turbidite.

The second type of lacustrine turbidite, LT2, is observed near the northern basin edge of lake Riñihue (Figures 2f and 7a). It consists of a nongraded heterogeneous mixture of detrital fine sand and particulate organic matter (Figures 7b and 7c). The composition, location, and extent of these turbidites show that they originated from subaqueous slope failures near a small alluvial fan at the lakeshore. This is corroborated by

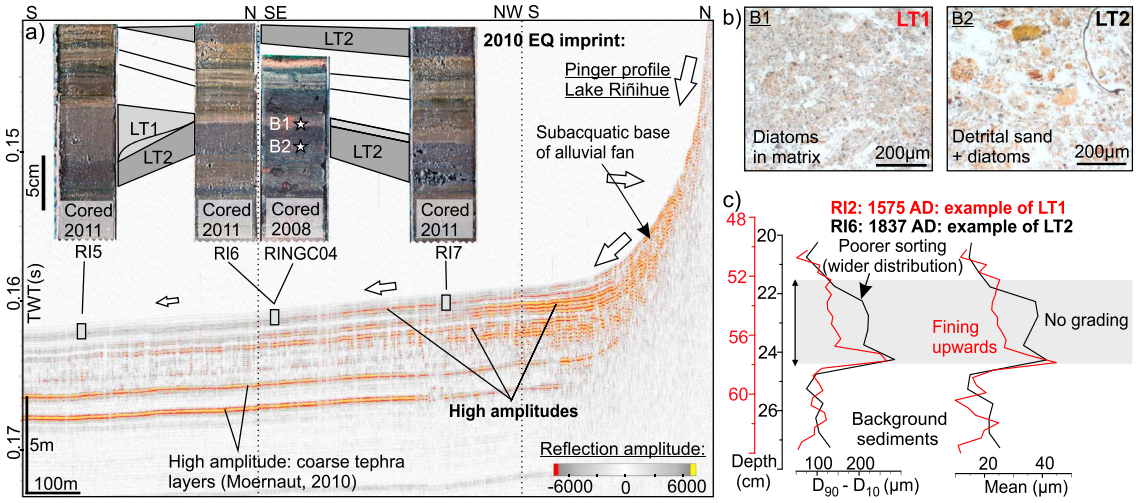

Figure 7. (a) Pinger profile (location Figure 2f) in lake Riñihue showing a decrease in reflection amplitude from the subaquatic base of an alluvial fan toward the basin plain. Comparison of cores taken in 2008 and 2011 (location: Figure 2f) indicates the presence and distal evolution of a lacustrine turbidite type 2 (LT2) originated at the subaquatic slopes of this alluvial fan during the 2010 earthquake. The older LT1 originated from a different (hemipelagic) slope in the NW of this sub-basin (see Figures 12 and 16i). (b) Thin section images of an LT1 and an LT2 associated to a single chronostratigraphic level. LT2s contain more and larger detrital grains than LT1s. (c) Comparison of grain-size characteristics (width of distribution and mean) of a typical LT1 and LT2 in cores RI2 and RI6 (details in Figure 12). LT2s show a higher mean grain size, poorer sorting, and less grading than LT1s. D_{90}, D_{10}: 90th and 10th percentiles of the grain-size distribution, respectively.

the basinward decrease of seismic-reflection amplitude (Figure 7a), probably caused by decreasing content of dense detrital LT2 sediment within the sequence. Patterns in grain size and MagSus do not always allow an unambiguous discrimination between LT1s and LT2s. Hence, the best criterion is the microfacies content, which shows a significant lower amount of diatoms and larger amount of detrital grains and particulate organic matter in LT2s compared to LT1s (Figure 7b).

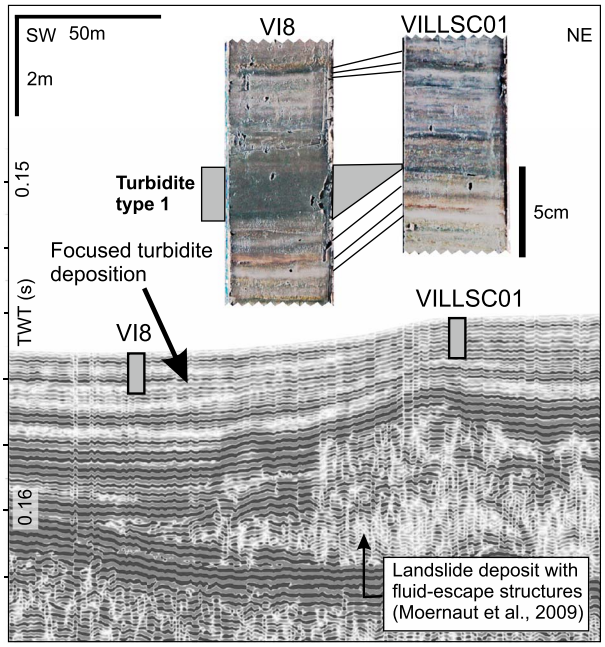

Figure 8. Pinger profile in Lake Villarrica (location Figure 2d) showing basin-focused sedimentation. Despite the sites' proximity, turbidites are much thicker in core VI8 than in VILLSC01 (see Figure 10 for the complete cores), indicating that turbidites are focused toward topographical lows.

The thickness and grain-size characteristics of a single turbidite vary as a function of the coring site location relative to the sediment source (Figure 5). Distally, turbidite deposits tend to be thinner and the sandy basal unit pinches out. In the most distal sites or at shallower locations, only the clayey top of the turbidite is present (e.g., uppermost turbidite in Figure 5). Moreover, the thickness of a single turbidite is also influenced by the exact pathways of the turbidity currents as determined by topographical gradients, and focusing of suspended sediments to bathymetric depressions results in much thicker turbidites (e.g., Figure 8). Therefore, detailed bathymetric info and multiple coring sites per sub-basin are generally required to obtain a relative estimate of the volume of the causative slope failures.

4.2. Age Models and Stratigraphic Correlations

The age-depth models (Figure 9) based on varve counting on one master core

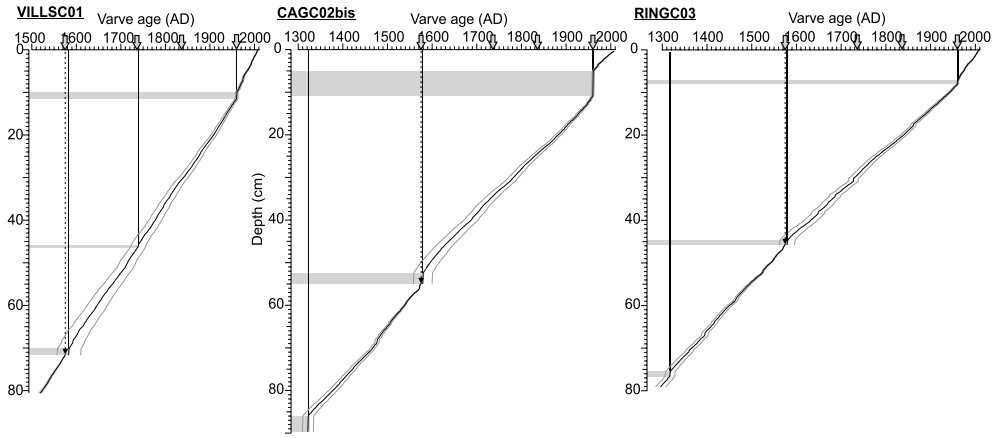

Figure 9. Age-depth models based on varve counting for VILLSC01, CAGC02BIS, and RINGC03. Turbidites (grey bars). Age of the major historical earthquakes along the VS (grey arrows). Retained medium age-depth model (black line). Error range for the age-depth model based on the average of the relative error between counting sessions (grey lines; see section 3.2). The 1575 earthquake and associated turbidite serve as a tuning point (dashed line with arrow) which largely reduces the error range for the lowermost sediments.

per lake show relatively constant sedimentation rates per lake, punctuated by lacustrine turbidites and volcanic event deposits. Average background sedimentation rate at VILLSC01 (~1.5 mm/yr) is higher than at CAGC02BIS (~1.0 mm/yr) and RINGC03 (0.9 mm/yr). Accurate core correlation between sub-basins in a lake (Figures 10–12) was primarily based on visual correlation of tephra-fall layers, lahar deposits, and color changes in the background sediments and confirmed by the correlation of MagSus patterns. Moreover, geochemical and mineralogical analysis of the most prominent tephra layers in the three lakes allowed the identification of three key tephrostratigraphic horizons represented by VT1/CT7/RT3, CT1/RT1, and VT2/CT9 (Figure 13), which allow interlake correlation. The VT1/CT7/RT3 assemblage has a very distinct geochemical signature with a relatively high K_2O to SiO_2 ratio and is likely related to a poorly documented eruption of the Huanquihue Volcano Complex located southeast of our study region [*Van Daele et al.*, 2014]. The medium varve ages of these tephra assemblages are 1594/1598/1592 for VT1/CT7/RT3 and 1956/1954 for CT1/RT1. The stratigraphic level of VT2/CT9 is not reached by the cores used for varve counting. The small age differences for a single assemblage lie within the cumulative error (±16–25 years around 1595 and ±2–3 years around 1955) of the repetitive varve counting procedure and suggest consistent varve age models for these different lakes. Intralake core correlation shows that large-scale erosion of sediment laminae below the turbidites is absent and confirms the continuity of the age-depth models. However, minor erosion of a few laminae may have occurred, accounting for some of the differences in varve age.

The intralake and interlake core correlation between 10 studied sub-basins demonstrates that multiple individual turbidites are present at distinct stratigraphic levels. The medium varve ages of the historical LT1s in the three lakes can be grouped within an age range of maximum nine years (Table 2) and correlate clearly with the main events of the historical earthquake record along the Valdivia Segment (1960, 1837, 1737, and 1575).

The 1960 and 1575 earthquakes are represented by LT1s in each studied sub-basin (Table 2). LT1s associated with the 1837 and 1737 earthquakes are present in respectively five and eight of the studied sub-basins and have a significantly smaller cumulative turbidite thickness per lake. This means that the 1837 and 1737 turbidites are generally thinner and travelled less far than the 1960 and 1575 turbidites (Figures 10–12). Due to uncertainty in varve counting, we cannot exclude the possibility that the turbidite dated around 1837 may in fact correlate with the 1835 event at the Maule Segment. However, we decided not to attribute turbidites to the 1835 event, because in Valdivia (39.8°S), the reported earthquake impact in 1837 was considerably larger (incomparable) than in 1835 [*Lomnitz*, 1970; *Cisternas et al.*, 2005]. In four sub-basins in lakes Villarrica and Calafquén, we found thin LT1s at the topmost part of cores taken in 2011, which shows that the 2010 M_w 8.8 earthquake at the Maule Segment left a relatively modest sedimentary fingerprint in our study region.

Subaqueous failures at an alluvial fan in lake Riñihue (LT2s) occurred more frequently (Figure 12) than failures at the lateral nondeltaic slopes (LT1s). Although nonseismic triggers for LT2s are not impossible (see

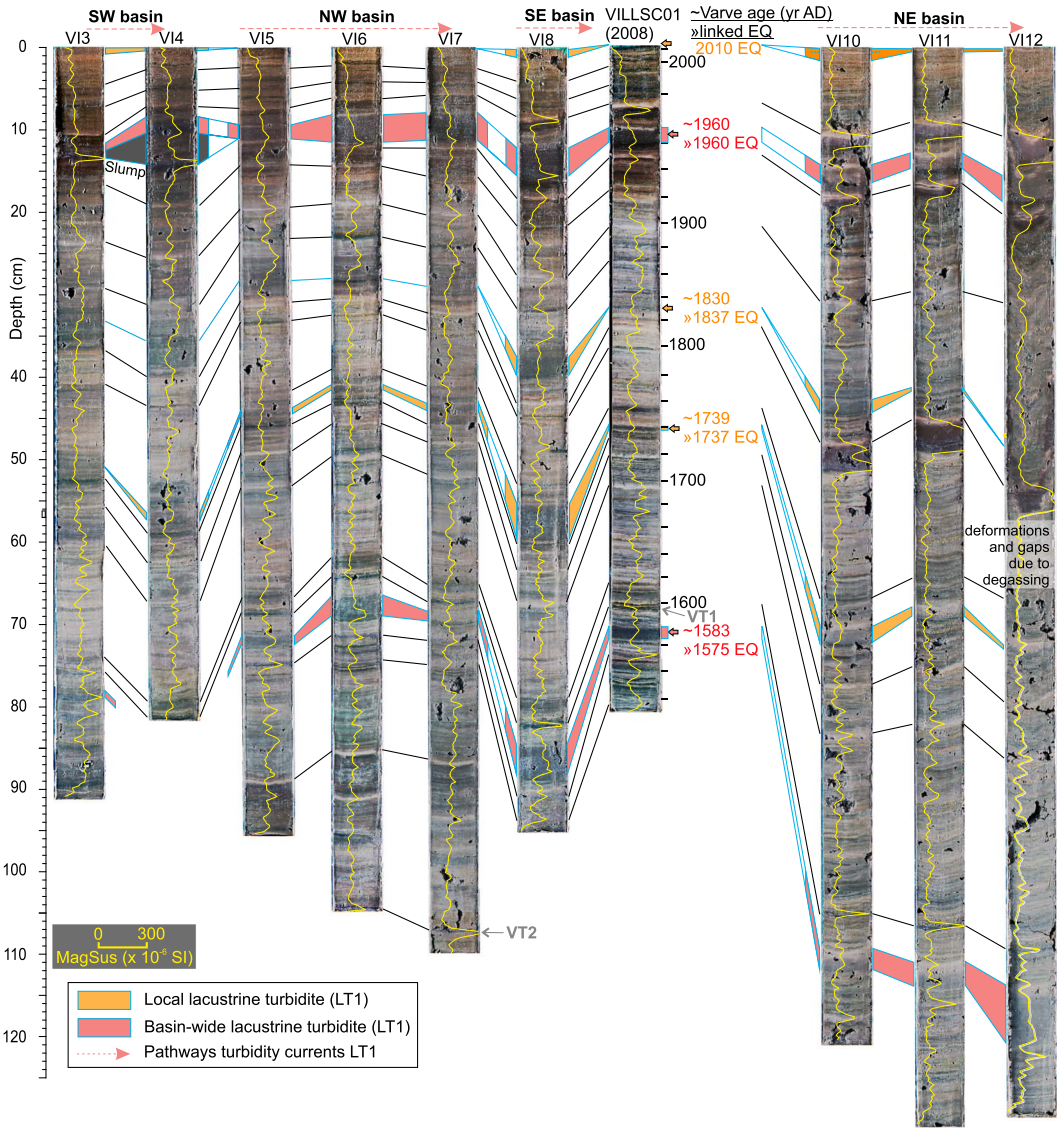

Figure 10. Core correlation and turbidite stratigraphy for four sub-basins in lake Villarrica. Key stratigraphic horizons used to correlate (based on sediment color and MagSus pattern; black lines). Stratigraphic level and extent of lacustrine turbidites (blue lines and color infill; see legend). For illustrative purposes, we give local LT1s a different color than basin-wide LT1s. Varve-counted age-depth model (not tuned) and linkage of lacustrine turbidites with historical earthquakes. Interrupted coloring marks individual turbidites deposited in separate sub-basins at the same time. Sampled tephra levels in grey (VTx).

section 2.2), we found a clear association of the LT2s in lake Riñihue and the main earthquakes of the Valdivia Segment (1960, 1837, 1737, 1575). Thinner LT2s also seem to correlate with the local intra oceanic plate earthquake in 1934 (M_s 7.1; varve age 1930 ± 3) and an earthquake in 1920 with unknown source mechanism (M_s 7.4; varve age 1918 ± 4). Moreover, an LT2 is present at the uppermost part of some Riñihue cores which were taken in 2011. As sediment cores at the same positions taken in 2008 do not show this LT2 (Figure 7), we can firmly attribute it to the 2010 Maule earthquake.

Two prehistorical multibasin turbidite events (Figures 11 and 12 and Table 2) were identified and dated by tuning the varve chronology to the 1575 earthquake. Three sub-basins show relatively thin turbidites at 1465 ± 5 (Calafquén) or 1467 ± 4 (Riñihue) and thicker turbidites at 1321 ± 11 (Calafquén) or 1317 ± 10 (Riñihue). Coring depth limitations hamper detection of equivalent turbidites in all 10 sub-basins.

Only seven turbidites out of the 54 turbidites lack a (chrono-) stratigraphic counterpart in the other basins and can be considered as "single" turbidites. These are relatively thin (< 2 cm), spatially more restricted, and

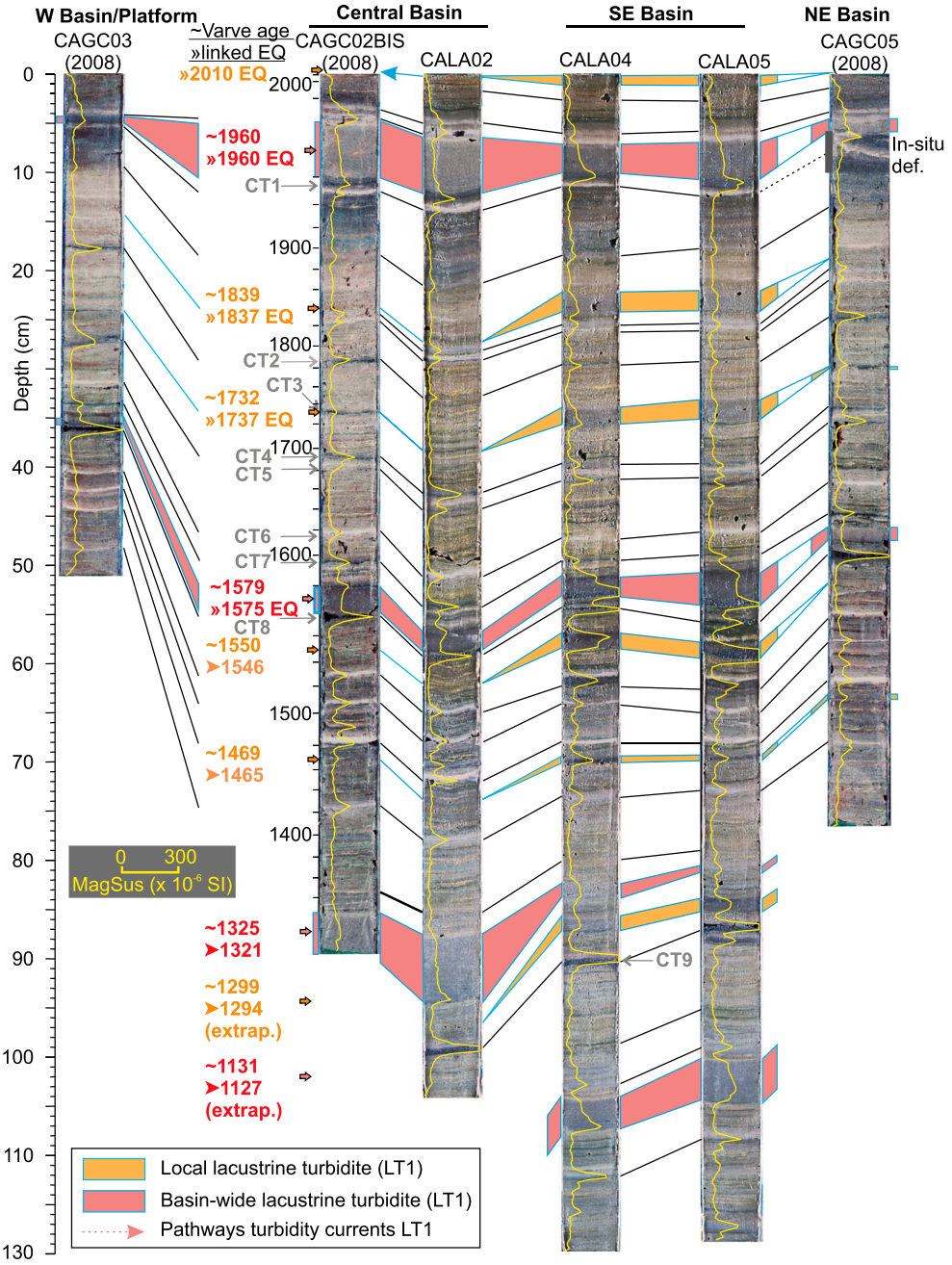

Figure 11. Core correlation and turbidite stratigraphy for four sub-basins in lake Calafquén. Line styles, colors, and age determination as in Figure 10. Pre-1575 varve ages are calibrated using the 1575 event as a tie point. Sampled tephra levels in grey (CTx).

are either located in the basin in front of the "alluvial fan" in lake Riñihue (LT2s: 1930 ± 3, 1918 ± 4, 1884 ± 5, 1604 ± 16) or the "southeast basin" in lake Calafquén (LT1s: 1546 ± 2, 1294 ± 14; Figure 11). In the latter basin, a much thicker (up to 4 cm) single turbidite was deposited in 1127 ± 44. Two of the single turbidites in Lake Riñihue were linked to the instrumentally recorded earthquakes in 1934 and 1920 (see above), so the other single turbidites may also have been created by local earthquakes in preinstrumental times. However, to confidently exclude a nonseismic origin (e.g., floods or onshore soil slides triggered by heavy rainfall), more detailed studies including high-resolution grain-size and microfacies analysis are needed.

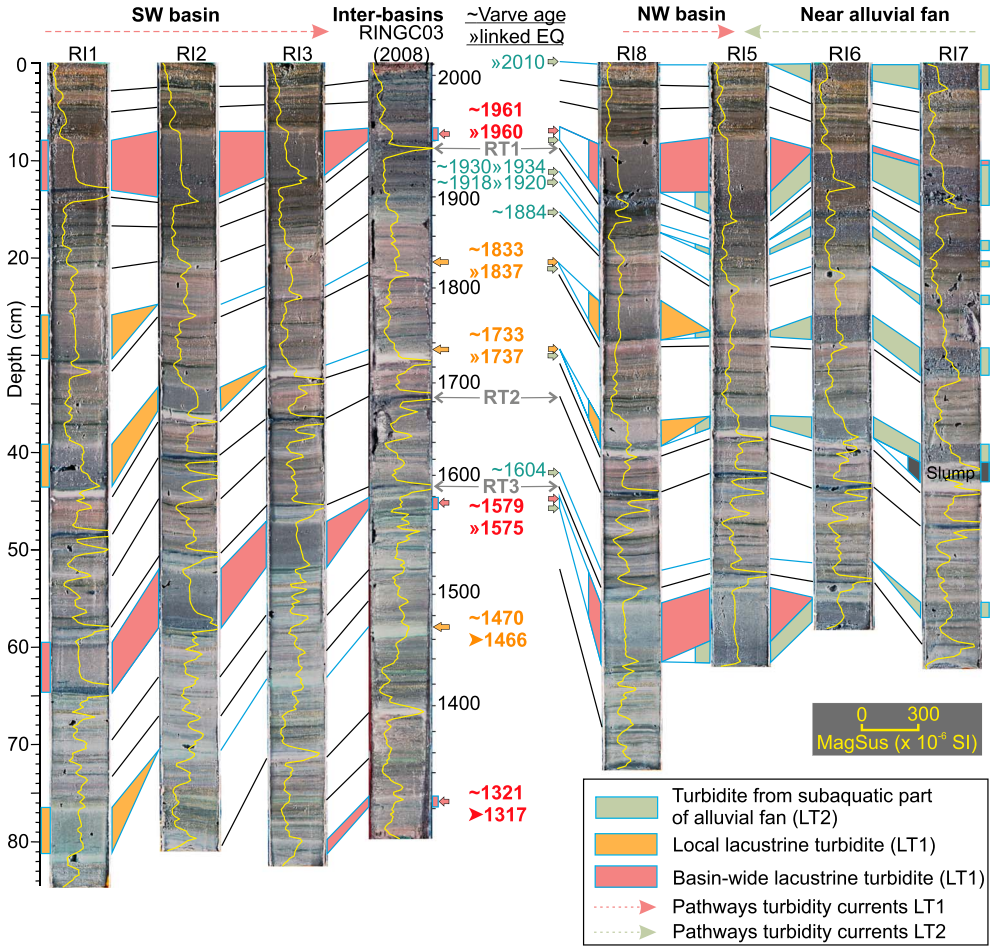

Figure 12. Core correlation and turbidite stratigraphy for two sub-basins in lake Riñihue. Line styles, colors, and age determination as in Figure 10. Pre-1575 varve ages are calibrated using the 1575 event as a tie point. Sampled tephra levels in grey (RTx).

5. Quantitative Lacustrine Paleoseismology

For the regional earthquake catalogue of the last 100 years, we obtained consistent results between the deduced seismic intensities (Table S1) and the triggering, type, and cumulative turbidite thickness (CTT) of lacustrine turbidites. This is best illustrated by the sedimentary archive of lake Riñihue (Figure 14a). Here hemipelagic slope failures (LT1s) and alluvial fan failures (LT2s) took place during the 1960 earthquake when seismic intensity was about VII½. Alluvial fan failures (LT2s) also occurred during the events of 2010, 1934, and 1920 when seismic intensities were between V½ and VI½. The alluvial fan remained stable during the event of 1975, which may have reached an intensity of almost VI there. This range of intensity thresholds (from V½ to VI) to create LT2s at this location may be a consequence of the cumulative error on instrumental earthquake data and attenuation formulae or by slight differences in local slope stability over time. Earthquakes with seismic intensities lower than V½ during the last 100 years did not leave any sedimentary fingerprint at our study sites. In the studied basins in lakes Villarrica and Calafquén, LT1s are only produced during the 2010 (seismic intensity VI¾ and VI½) and 1960 events (intensities of VII½) as no significantly large alluvial fans are present to allow for LT2 generation. The 2010 event—having a southward decrease of seismic intensity in our study area—induced slope failure of the hemipelagic slopes in three sub-basins in lake Villarrica (39.3°S), while at lake Riñihue (39.8°S), it was not strong enough to form an LT1.

Interestingly, the cumulative turbidite thickness of the LT2s in Lake Riñihue seems to correlate with seismic intensity values (Figure 14b), suggesting that the amount of sediment involved in the turbidity currents may be directly influenced by the local seismic intensity of the causative earthquake. This inference is

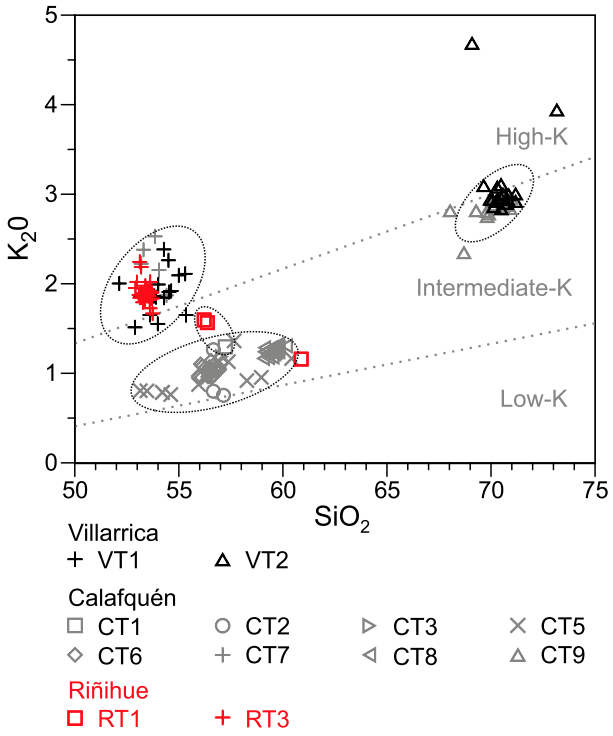

Figure 13. K_2O versus SiO_2 (wt %) variation diagram of glass shard compositions in the analyzed tephra fallout deposits in lakes Villarrica (black; sample location in Figure 10), Calafquén (dark grey; sample location in Figure 11), and Riñihue (red; this study; sample location in Figure 12). The data of lake Villarrica and lake Calafquén are derived from *Van Daele et al.* [2014]. Distinct assemblages are formed by VT1/CT7/RT3, CT1/RT1, and VT2/CT9.

supported by the comparable CTT in all three lakes associated to the 1960 and 1575 earthquakes, the reported effects of which were very similar at the latitude of Valdivia [*Lomnitz*, 1970; *Cisternas et al.*, 2005]. In comparison, effects of the 1837 and 1737 earthquakes were more modest there and are represented by less extensive turbidites having a lower CTT. One may suppose that the amount of sediment involved in the turbidity current is strongly dependent on the time elapsed since the last turbidite event (memory effect) and relates to the amount of potentially unstable sediment accumulated on the slopes since then. However, at first sight, no such relationship emerges from our records. For example in lake Riñihue, the turbidity currents produced in 1737 were relatively small although they ended the largest interevent time interval in the records there (1575 to 1737: 162 years). We assume that most of the documented turbidites in our lakes are created by rather superficial slope failures (< 1 m thick) based on the relatively modest dimensions of slide scars on the slopes and most landslide deposits in the sub-basins (Figure S2). The recurrence of such shallow slope failures is much less influenced by slope sediment accumulation rates than is documented for large-scale slope failures involving the evacuation of several meters of slope sediment [e.g., *Strasser et al.*, 2011]. Furthermore, relative constant background sedimentation rates (Figure 9) for the studied time interval allow for continuous replenishment of slopes and comparable consolidation profiles of shallow sediments at different times. This would result in turbidite records which are principally free of "memory effects," a finding that has been

Table 2. Summary of the Lacustrine Turbidite Stratigraphy and Correlation to Historical and Prehistorical Earthquakes at the VS (Except the 2010 Event at the MS)[a]

Earthquake (year A.D.)	Varve Age of Associated Stratigraphic Level (year A.D. ± error)			Relative Number of Sub-basins with LT1s				CTT of LT1s (cm)				CTT LT2s (cm)
	Vill	Cal	Riñ	Vill	Cal	Riñ	All Lakes	Vill	Cal	Riñ	All Lakes	Riñ
				Historical								
2010 (MS)	Core top	Core top	Core top	3/4	1/2	0/2	4/10	4.4	5.5	0	9.9	4.4
1960	1960 (±3)	1960 (±2)	1961 (±2)	4/4	4/4	2/2	10/10	23.6	25.1	29.1	77.8	9.4
1837	1830 (±10)	1839 (±8)	1833 (±7)	2/4	1/4	2/2	5/10	3.8	4	8.6	16.4	5.9
1737	1739 (±16)	1732 (±14)	1733 (±11)	4/4	2/4	2/2	8/10	11.1	3.7	9.6	24.4	5.2
1575	1583 (±25)	1579 (±21)	1579 (±17)	4/4	4/4	2/2	10/10	22.4	15.2	29.2	66.8	*4.5*
				Prehistorical								
~1466 (±4)	-	1465 (± 5)	1467 (±4)	-	2/4	1/1	-	-	*2.7*	*4.6*	-	-
~1319 (±9)	-	1321 (±11)	1317 (±10)	-	2/2	1/1	-	-	*18.4*	*4.4*	-	-
~1127 (±44)	-	1127 (±44)	-	-	1/1	-	-	-	*7.4*	-	-	-

[a]For each grouped event, its varve age (with relative error), the amount of sub-basins with LT1 evidence, and the cumulative turbidite thickness are given. We document LT2s only for lake Riñihue. The ages of the prehistorical earthquakes are the mean values of the varve ages for these events, which are tuned to the 1575 event (see section 3.2). In lake Calafquén, not all sites were resampled in 2011, so the relative presence of turbidites triggered in 2010 is not correct. Hyphens indicate stratigraphic level not reached by the cores. Italic numbers indicate not all cores reached this stratigraphic level, so the presented value may be significantly underestimated.

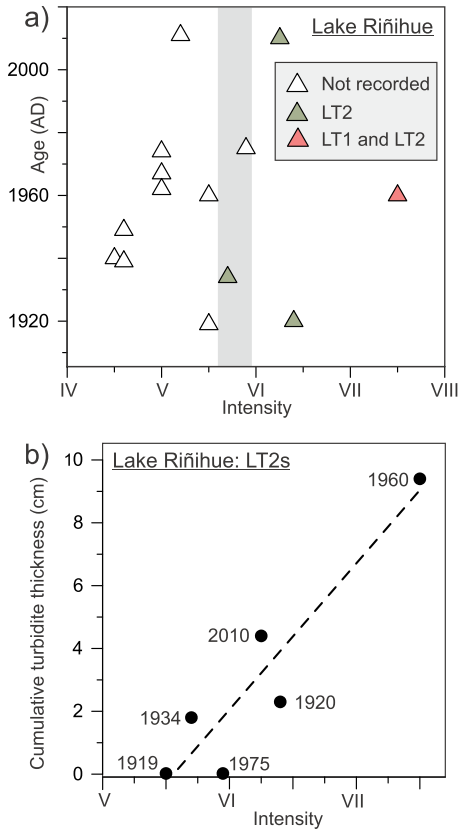

Figure 14. Calibration of lacustrine turbidites in lake Riñihue with seismic intensities for the main (instrumentally recorded) earthquakes of the last 100 years near the study region. (a) Absence/presence of associated LT1s and LT2s in the sedimentary archive for each earthquake. Empirically derived lower seismic intensity threshold (~V½-VI) for LT2 generation in the studied basin in lake Riñihue (grey range). (b) Suggested linear correlation between CTT for LT2s and seismic intensity of the causative earthquakes.

statistically justified for several marine turbidite records in different settings [*Clare et al.*, 2014].

Assuming that turbidite size correlates to local seismic intensity, we will estimate the seismic intensity values of preinstrumental earthquakes by putting their normalized, weighted cumulative turbidite thickness (see section 3.4) within a linear framework obtained from the seismic intensity and CTTs associated to the well-documented 2010 and 1960 earthquakes (Figure 15). For these events, reported intensity values were compiled in a reliable and systematic way. We do not include the 1934 or 1920 earthquakes in the framework as we only found their imprint in lake Riñihue and their intensity estimates may be significantly flawed by uncertainties related to their hypocentral location, magnitude, and the used attenuation curves (see section 3.3).

Using this linear framework, the very similar LT1 thickness pattern for the 1960 and 1575 in all lakes results in intensities of about VII½ (Figure 15). For the 1737 and 1837 events, thickness values for LT1s in lake Villarrica culminate at 15–50% of the 1960 LT1s, which represent seismic intensities between VI½ and VII. In lakes Calafquén and Riñihue, LT1 thickness values for the 1837 and 1737 events are around 15–20% of those for the 1960 event and relate to intensities averaging at VI½ (Figures 15a–15c). Additionally, seismic intensity estimates for the LT1s (VI½) in lake Riñihue are strikingly similar (Figures 14c and 14d) to those for the LT2s, which means that our approach may be used for both turbidite types. Moreover, two unknown local earthquakes around 1884 and 1604 with relatively small intensities of about V½ were revealed by LT2s in lake Riñihue. In summary for all studied lakes, basin-wide turbidites type 1 record seismic intensities ≥VII½, while local turbidites type 1 are produced by seismic intensities of VI½ to VII. Subaqueous failures of the alluvial fan in Lake Riñihue can even be initiated by seismic intensities as low as V½. Lower intensities—produced by small, local earthquakes, or distant great earthquakes—did not produce any sedimentary imprint at our coring sites.

In some cases, relative turbidite thickness at a single coring site seems not to be representative for the earthquake's seismic intensity. For example, the 1575 turbidite in core VI7 is much thinner than the 1960 turbidite, while the inverse is observed in core VI12 (Figure 10). Such differences can be caused by the location and amount of earthquake-triggered landslides bringing sediment in suspension, or temporal variations in the slope sequence lithology (and consolidation) affecting the volume of sediment remobilization. Therefore, comparison of the thickness and spatial extent of turbidites in multiple basins is crucial for quantifying the seismic intensity of paleoseismic events. If for any reason the number of studied sub-basins for a specific stratigraphic level is limited, turbidite thickness patterns become thus less reliable for paleoseismic intensity estimation. Alternatively, the presence or absence of turbidites at each site can be used to estimate a site-specific earthquake-recording threshold (EQRT). The EQRT at an individual coring site corresponds to the seismic intensity that needs to be reached in order to deposit a lacustrine turbidite at that specific site. The EQRT is primarily influenced by the distance of the sediment core to the source area

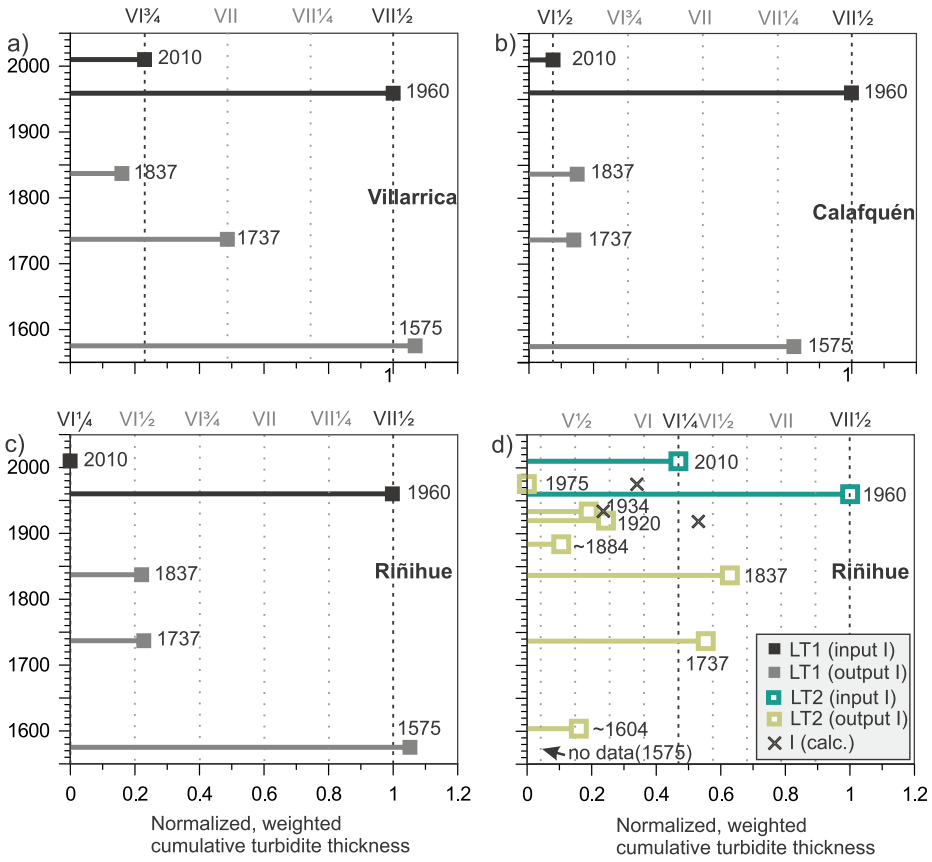

Figure 15. Calculation of seismic intensity for historical earthquakes (in dark grey and light green) based on cumulative turbidite thickness (CTT). The reported seismic intensity (I) values and CTT of the 2010 and 1960 events are used as input parameters (in black and dark green). CTT is normalized to the 1960 event values and analyzed per sub-basin, in this way representing relative differences in the CTT of each turbidite. The plots represent the average value (over all sub-basins) per event for each studied lake. (a–c) LT1s in lakes Villarrica, Calafquén, and Riñihue show clear differences in terms of inferred intensity between the 1960/1575 events and the 2010/1837/1737 events. (d) LT2s in lake Riñihue. For the 1975, 1934, and 1920 events, the seismic intensity values based on attenuation formulae applied on instrumental earthquake data are also shown.

of the turbidity current (e.g., Figure 5) and the minimum seismic intensity needed to induce sediment remobilization there. For the prehistorical turbidites in our lakes, core length was insufficient to reach the desired stratigraphic levels in all cores, and thus, the cumulative turbidite thickness is underestimated. Therefore, we determined the EQRT for each coring site (Figures 16g–16i) based on the presence/absence of historical turbidites (Figures 16d–16f) and the seismic intensity of the causative earthquakes at each lake (Figures 16a–16c), which is either reported in literature or inferred via the calibrated historical turbidite records. The EQRT at the coring sites is then used to estimate the seismic intensity for the prehistorical earthquakes. Due to its specific location at the merging point of turbidite pathways, core RI5 in the northern basin of lake Riñihue holds a hybrid paleoseismic record that recorded I ≥ V¾ as LT2s and I ≥ VII½ as LT1s.

The inferred EQRT at those sites in lakes Riñihue and Calafquén where a turbidite was created in ~1466 points to a seismic intensity of about VI½ (similar to the 1837 and 1737 events). This seismic intensity value is further constrained by the absence of a coeval turbidite in the NW basin of lake Villarrica where the EQRT is about VII. The turbidites associated to an event in ~1319 reached a site of EQRT = VII½ in both lakes Riñihue and Calafquén, which makes its impact very similar to the giant earthquakes of 1960 and 1575. Due to coring limitations, the turbidite in ~1127 could only be identified in the SE basin of lake Calafquén, where an EQRT of VI½ is inferred. Its thickness is slightly larger than the 1960 and 1575 turbidites, and much larger (double or more) than the 2010, 1837 and 1737 turbidites, or the other single turbidites (see section 4.2). Therefore, we suggest that the ~1127 event may have had a seismic intensity similar to the 1960 event (VII½) or even higher, although—with only one recorded turbidite—the uncertainties are much higher.

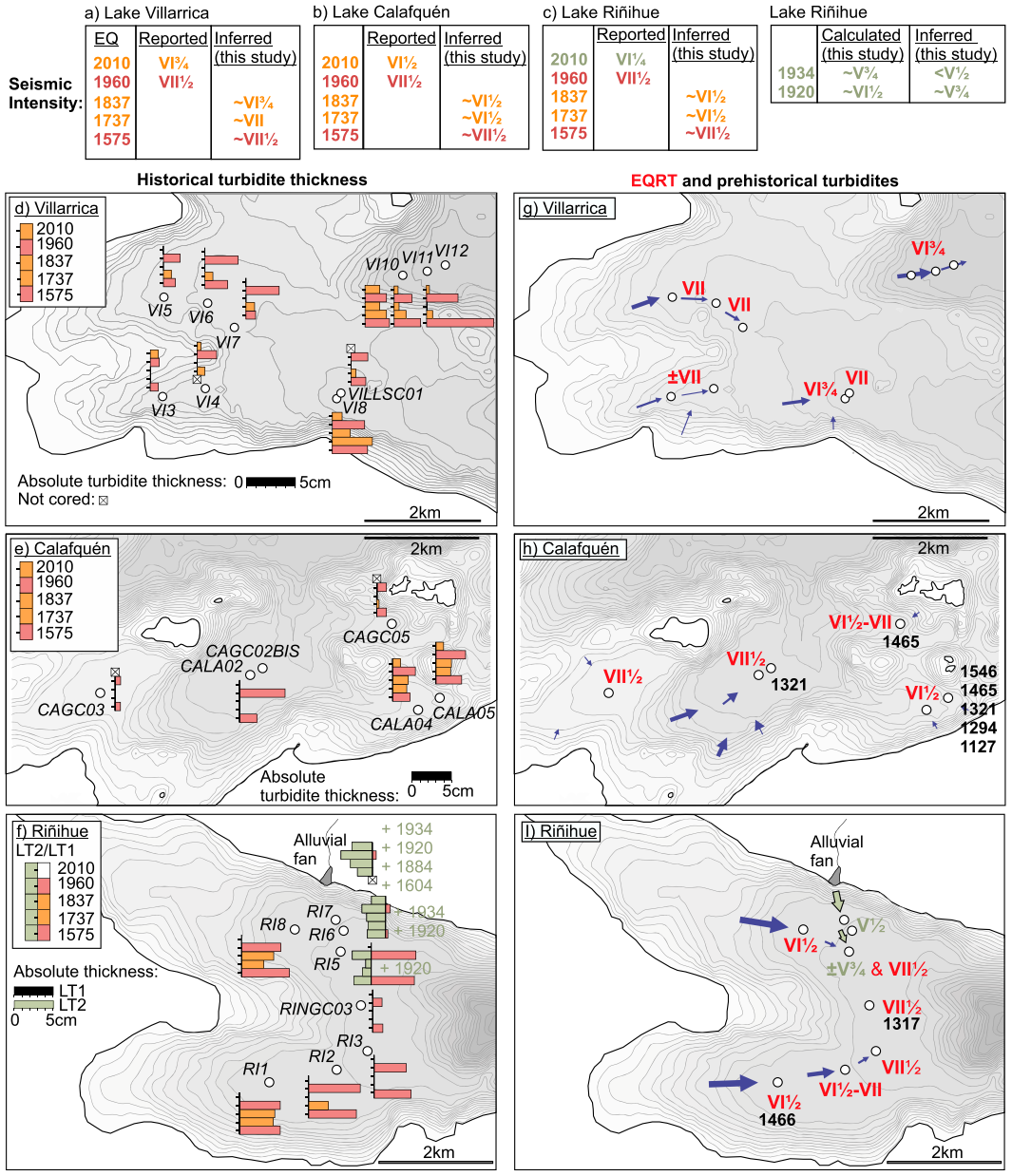

Figure 16. (a–c) Reported seismic intensity at each lake for the 2010 [*U.S. Geological Survey*, 2010] and 1960 [*Lazo*, 2008] events. Inferred seismic intensity at each lake for the 1837, 1737, and 1575 events (this study) based on the correlation of CTT and seismic intensity (Figure 15). The seismic intensity values for the 1934 and 1920 events are calculated via instrumental earthquake data. (d–f) Bathymetry of study areas (isobaths: 10 m) with the thickness of lacustrine turbidites at each coring site (horizontal bars) for the five considered stratigraphic levels ((top to bottom) 2010, 1960, 1837, 1737, and 1575). Core locations in italic. Basin-wide LT1s in red, local LT1s in orange, and LT2s in green. Ages near the alluvial fan in lake Riñihue represent additional LT2s in these coring sites. (g–i) Earthquake-recording threshold (EQRT; in Roman numerals) at each coring site for registering LT1s (all lakes) and LT2s (in case of lake Riñihue) based on the presence/absence of historical turbidites (Figures 16d–16f) and the intensity of their causative earthquakes (Figures 16a–16c; see text). Prehistorical turbidite evidence (plotted ages in black) is fragmentary as only a few cores reach sufficiently far back in time. Arrows indicate the assumed direction and volume of sediment transport.

6. Discussion

6.1. Causative Faults for Earthquake-Triggered Turbidites

The one-to-one correlation of lacustrine turbidites of type LT1 (i.e., similar to the background sediments) with the strongest historical earthquakes suggests that LT1s in the studied sub-basins were exclusively produced

by earthquake shaking. Due to the characteristic sedimentary content of LT1s and their synchronous triggering in multiple isolated basins, other triggering mechanisms for slope failure and turbidity currents can be ruled out (see section 2.2). Although megathrust earthquakes are the most frequent events causing high seismic intensities in Chile [*Leyton et al.*, 2010], the role of more local earthquakes—such as continental-crust earthquakes or events within the subducting oceanic slab—should also be evaluated as potential triggers for lacustrine slope failure.

In our study region, the Liquiñe-Ofqui Fault Zone (LOFZ) is made up of a complex structural pattern of individual N-S and NW-SE lineaments and second-order structures such as horsetails, tail cracks, splays, and pull-apart basins [*Rosenau et al.*, 2006]. Due to this segmentation, we do not expect this part of the LOFZ to produce major earthquakes ($M_w > 7$). Nevertheless, an event comparable to the 2007 Aysén earthquake (M_w 6.2; Figure 1) could produce maximum intensities of VII at our coring sites (≥25 km from LOFZ trace) and possibly leave a turbidite type 1 there, but—due the limited spatial impact of such events—only at one of our studied lakes at a time. At the Aysén Fjord, it is hypothesized that another three to four similar events took place during the Holocene [*Van Daele et al.*, 2013]. In our study region, which is close to the northern termination of the LOFZ, slip rates are significantly smaller than at the Aysén Fjord [*Wang et al.*, 2007], so an even lower occurrence of significant LOFZ earthquake events can be expected.

Intermediate-depth earthquakes in the subducting oceanic slab of Chile can reach magnitudes up to M_s 8 and can produce seismic intensities up to *X* (e.g., the 1939 M_s 7.8 earthquake in Chillán; Figure 1b) [*Beck et al.*, 1998]. Probably, a smaller oceanic slab event in 1934 (M_s 7.1; I = V¾) created an alluvial fan failure in Lake Riñihue (LT2), but no failure of hemipelagic nondeltaic slopes. In the region of Santiago, M_s 6–7 intraoceanic slab events occur about three times less frequently than interplate earthquakes of the same magnitude [*Leyton et al.*, 2010]. Compared to the largest megathrust events, they have a much shorter shaking duration, which is considered as an important factor for slope instability [*Ten Brink et al.*, 2009]. For our study area, the probability of large oceanic slab earthquakes has not been determined yet, making it difficult to estimate their potential contribution to the lacustrine turbidite records.

Volcano-tectonic earthquakes are generally of much lower magnitude ($M_w < 3$) [*Zobin*, 2001] and intensity, and no lacustrine turbidites correlate with the historical eruption history of Villarrica Volcano [*Van Daele et al.*, 2014]. Very rarely, large caldera collapses can take place at a volcano and produce a large earthquake (M_w up to 7) [*Zobin*, 2001]. The last caldera collapse at Villarrica Volcano took place around 3.6–3.8 ^{14}C kyr B.P. [*Silva Parejas et al.*, 2010], which is beyond the time span of our study.

We cannot fully exclude the most significant intraoceanic slab, LOFZ, and volcanic earthquakes as potential triggers for lacustrine slope failure in prehistorical times, but as their area of impact is typically much smaller than for megathrust events, latitudinal transects of paleoseismic records should be able to discriminate interplate earthquakes from these more local and much more infrequent events. In the following sections, we discuss scenarios for megathrust earthquakes only, as these are predominantly recorded in our lacustrine archives and are represented by turbidites in multiple lakes.

6.2. Implications for MS Earthquake History

Our newly established, calibrated paleoseismic information from lake sediments allows further improvement of the historical earthquake catalogue of south central Chile. The 2010 Maule earthquake, an event located along the MS, was recorded in the lacustrine sequences as far south as lake Riñihue (39.8°S). Its calibrated turbidite record clearly shows a latitudinal gradient associated with the northern location of the 2010 rupture compared to the studied lakes. Other large historical earthquakes along the MS, the shaking and tsunami of which were damaging at Concepción, did not leave any sedimentary trace at our coring locations. This might suggest that the 2010 event was much stronger or ruptured further south than its predecessors. However, at Mocha Island (38.4°S; Figure 1), located at the southern tip of the 2010 rupture, coseismic uplift was slightly larger in 1835 than in 2010 (0.6 m versus 0.2–0.5 m) [*Kelson et al.*, 2012]. Also, many similarities between the 1751 and 2010 events were found by compiling historical accounts [*Udías et al.*, 2012], and thus, it seems that the 2010 earthquake rupture was not exceptional in size or southward extent.

Remarkably, the largest recorded peak ground acceleration (PGA: 0.93 *g*) for the 2010 event took place in Angol (37.8°S, 72.7°W) [*Boroschek et al.*, 2012] and not in the areas where most coseismic slip occurred (Figure 1). Such enhanced ground motion values away from the rupture area in southeastern direction may

explain why the 2010 event left a significant sedimentary imprint at the studied lakes whereas previous MS events (e.g., 1751) did not. Consequently, we speculate that the older MS events could have had similar rupture areas, but a different slip evolution in space and time, and hence no particular focusing of seismic ground motion toward our study region.

6.3. Implications for VS Earthquake History

The calibrated lacustrine turbidite stratigraphy suggests that the 1960 and 1575 events along the VS had similar intensities (I ≥ VII½) around 39.5°S and that shaking in 1837 and 1737 was significantly weaker, with seismic intensities of VI½ to VI¾ in 1837 and VI½ to VII in 1737. This implies that coseismic slip at this latitude was considerably lower than in 1960 (30–40 m) [*Moreno et al.*, 2009] or in 1575. In lake Villarrica, the 1837 earthquake imprint (i.e., relative number of turbidites and cumulative turbidite thickness) is smaller than the 1737 imprint (Table 2), whereas both events have a very similar imprint in lakes Calafquén and Riñihue. This latitudinal gradient in the relative magnitude of the 1837 and 1737 turbidites may point to a more southern location of the 1837 event but is not conclusive on its own.

The lacustrine data are in good agreement with the historical reports [*Cisternas et al.*, 2005] and the two main paleoseismic records in the region: the megaturbidite stratigraphy in the Reloncaví Fjord [*St-Onge et al.*, 2012] and the coastal record of tsunamis and coseismic subsidence at the Maullín River site (Figure 17a) [*Cisternas et al.*, 2005]. Both show extensive evidence for the 1960 and 1575 events which—combined with the lacustrine data—can be considered as very similar full ruptures of the VS with large (15–40 m) coseismic slip.

The 1837 event is present as a thinner turbidite in the Reloncaví Fjord [*St-Onge et al.*, 2012] and historical records (subsidence, tsunami) suggest that it ruptured at least the southern half of the VS. The reported "rather strong" shaking in Concepción [*Cisternas et al.*, 2005] may suggest that it extended even north of our study area (39.5°S). In any case, coseismic slip (if present) in the northern half of the VS must have been much smaller than in 1960, according to the modest lacustrine fingerprint, representing a seismic intensity of only VI½. The smaller transported mass at the Reloncaví Fjord and the absence of tsunami/subsidence at Maullín suggest less coseismic slip than in 1960 (25–30 m) [*Moreno et al.*, 2009] at the central part of the VS. Back-calculation via the reported M_t of 9¼ [*Abe*, 1979] for an inferred rupture length of 500–700 km [*Stein et al.*, 1986] results in an average coseismic slip value of about 13–18 m (see section 3.4) [*Nishenko*, 1985]. On the other hand, back-calculation via the inferred intensities based on the lacustrine record provides an M_s of 7.2 to 8.5, depending on the northern rupture termination of the 1837 event (~39°S to 41.5°S, respectively).

The presence of lacustrine turbidites for the poorly reported 1737 event and the absence of a turbidite at Reloncaví Fjord or tsunami/subsidence at the Maullín River suggest that it was a less extensive rupture located near Valdivia (~39–41°S). As no tsunami was reported at the latter locality, fault slip may have been significantly lower than, e.g., during the tsunamigenic (M_w: 8.8) 2010 event (10–15 m; Figure 1). We interpret that the 1737 event with an estimated M_s of 7 ¾ [*Lomnitz*, 1970] was comparable in size to the instrumentally recorded M_s 7.8 Valparaíso earthquake in 1985 which had an inferred rupture length of about 140 km and an average slip of about 1.7 m [*Barrientos*, 1988]. Back-calculation via the intensities derived from the turbidite stratigraphy results in an M_s value for the 1737 event of about 7.2–7.5 (see section 3). In the years following 1737, large earthquakes farther south at the Chonos Archipelago (1742, 43.8–45.8°S) and Chiloé Island (1748, 41.8-43.4°S) were reported [*Lomnitz*, 1970]. Although historical reports for this period are very scarce and spatially deficient, we speculate that these earthquakes represent adjacent interplate ruptures of similar size than the 1737 rupture area.

The discrepancies between the absolute values of our back-calculations and magnitude estimates in literature can be further explained by the large uncertainties in the input parameters of both models. This includes, for example, the assumed equivalence of magnitude and seismic intensity scales and the subjectivity when reporting earthquake damage [*Lomnitz*, 1970]. Therefore, the obtained values should mainly be considered approximate. Nevertheless, all studies indicate a large difference between, e.g., the 1837 and 1737 events in terms of magnitude, rupture extent, and coseismic slip.

6.4. Prehistorical Earthquakes

Since each studied sub-basin (Table 2) contains both the 1960 and 1575 turbidites, the lacustrine paleoseismic records for intensities of VII½ and more can be considered continuous and reliable (i.e., no under-recording of similar-size earthquakes). The prehistorical turbidites in lakes Riñihue and Calafquén around 1319 (±9) and

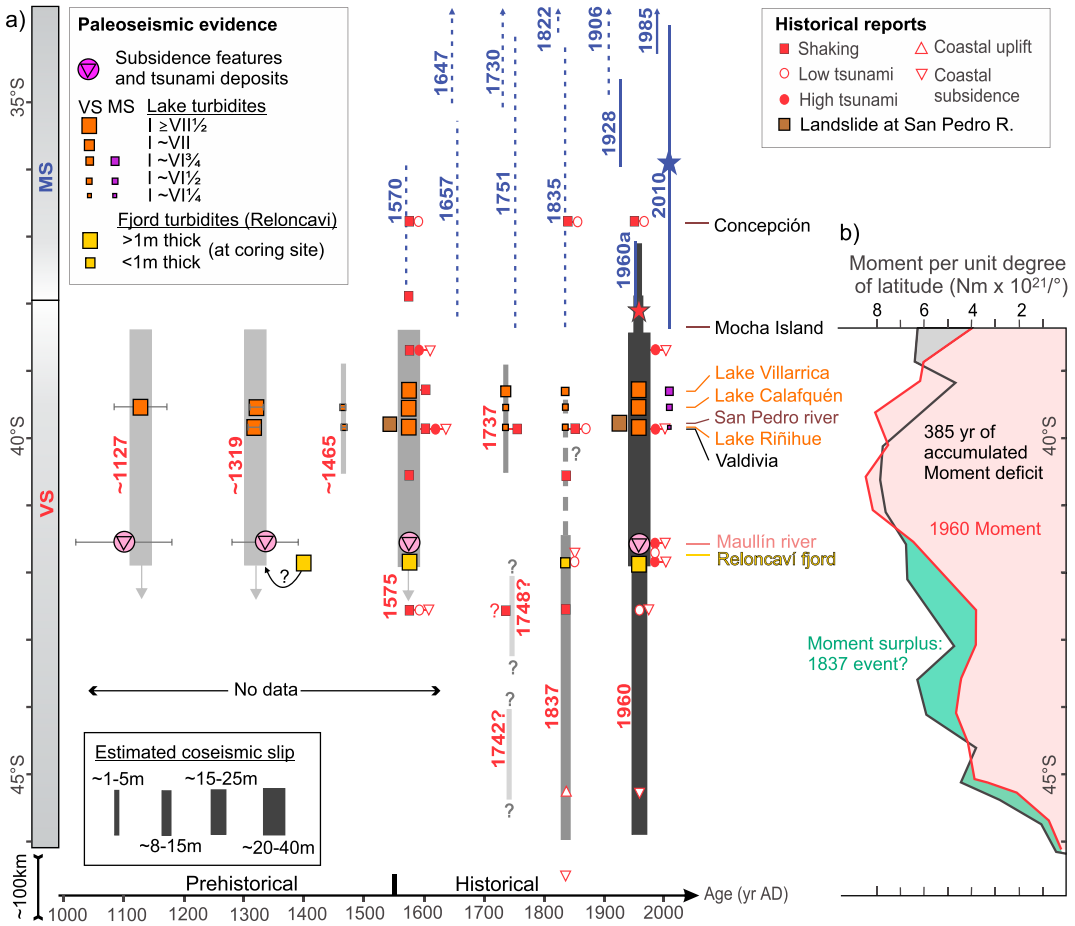

Figure 17. (a) Proposed variable rupture model for the main events at the VS based on a compilation of our lake records, historical, and paleoseismic data [*Cisternas et al.*, 2005; *St-Onge et al.*, 2012] and back-calculation of earthquake parameters (see text). This model includes rupture extent (position of grey bars) and coseismic slip (width of grey bars). Grey shading indicates the reliability of the reconstruction (weak (light); strong (black)). Question marks represent the uncertainty about some rupture limits. Small local earthquakes (e.g., 1975, 1934, 1920, etc.) are not included in the reconstruction. Pre-2010 ruptures at the MS are plotted based on a compilation from *Udías et al.* [2012] and *Melnick et al.* [2009, 2012], giving most weight to the most recent publications. (b) Latitudinal distribution of the coseismic moment of the 1960 event (red line), and the accumulated moment deficit (black line) due to 385 years (i.e., 1575-1960) of interseismic strain buildup at the plate interface at the Valdivia Segment [after *Moreno et al.*, 2011]. Interseismically accumulated moment surplus in the southern half of the VS when subtracting the 1960 coseismic moment (green area). This surplus may have been accommodated by the 1837 earthquake (see section 6.5). The area north of 39°S—where the MS and VS overlap—has a more complex history of strain buildup and release [see *Moreno et al.*, 2011; *Melnick et al.*, 2012] and is not the scope of our study.

1127(±44) are inferred to represent mega earthquakes of comparable shaking impact at this latitude. This interpretation is reinforced by the fact that the four major lacustrine turbidite events correlate with the uppermost events of tsunami and subsidence at the Maullín River site, two of which relate to the historical 1960 and 1575 events and two of which were radiocarbon dated (calibrated; 2σ age) at 1280–1390 and 1020–1180 (Figure 17a) [*Cisternas et al.*, 2005]. Possibly, the megaturbidite in the Reloncaví Fjord deposited around 1400 [*St-Onge et al.*, 2012] can also be associated to the 1319 (±9) event, but more accurate dating is needed. Both our lacustrine turbidite records—representing seismic shaking at ~39.5°S—and the record of tsunami and coseismic subsidence at 41.5°S [*Cisternas et al.*, 2005] provide a continuous record of the predecessors of the 1960 megathrust earthquake. Yet our new data set at quasi-annual resolution narrows dating uncertainties in the order of 100 years (^{14}C dates) to only a few years to decades. Moreover, multiple turbidites in our records reveal a new significant paleo-earthquake around 1466 (±4). Its inferred seismic intensity (VI½) and negative evidence at Reloncaví Fjord and Maullín River suggest that it was very similar in size and location than the historical 1737 event.

6.5. Variable Rupture Model

Coseismic slip in 1960 was much smaller south of 41.5°S (15–25 m) than in the northern half of the rupture (25–40 m; Figure 1) [*Moreno et al.*, 2009], a pattern which cannot be explained by the present locking distribution along the interplate megathrust [*Moreno et al.*, 2011]. *Moreno et al.* [2011] compared the 1960 slip values, general plate convergence rate, and interplate locking rate to the average interseismic time (300 years) of giant earthquakes in the VS and concluded that the 1960 event overspent some seismic moment in its northern half while releasing more or less the exact accumulated moment deficit in its southern half. However, when considering the real interseismic time between the giant earthquakes of 1575 and 1960 (385 years), a better match between interseismic and coseismic moment appears in the northern half of the VS and a surplus of interseismic moment exists in the southern half (Figure 17b). Assuming that interseismic strain buildup is purely elastic (i.e., no permanent deformation), this misfit can be explained by the assumption that the 1837 event released this "additional" accumulated interseismic strain in the southern half of the VS. In the northern half of the VS, the budget of accumulated and coseismic moment does not allow significant slip (more than several meters) during the 1837 event. In our study region, this is supported by the rather modest lacustrine fingerprint and the absence of river-blocking landslides at San Pedro River. Still, the compiled data do not allow constraining the northern rupture end in a decisive manner (Figure 17, dashed line). The hypothesized southern location of most of the 1837 moment release is in line with the locations of historically reported subsidence and tsunami in 1837, but its inferred average slip (~13–18 m) is too large (factor 1.5–3) to account for the leftover accumulated moment deficit. However, absolute values for the hypothetical coseismic moment in 1837 cannot be determined in a reliable way due to many uncertainties in the 1960 slip distribution and possible time-variability between the "present-day" interplate locking distribution (used in the moment budget calculation) and the one during the previous seismic cycle [*Moreno et al.*, 2011]. Also, we assumed that the 1575 earthquake released all accumulated interseismic strain (i.e., moment budget starts at zero) which, in general, is not necessarily the case during the seismic cycles of subduction megathrusts [*Goldfinger et al.*, 2013].

In the southern half of the VS, the thermally defined seismogenic zone extends close to the trench [*Völker et al.*, 2011], although the coseismic slip reconstruction for the 1960 event does not resolve any slip in this area [*Moreno et al.*, 2009]. If the 1837 event did rupture and release accumulated strain in this near-trench area, this would have significantly increased the efficiency of tsunami generation (tsunami earthquakes) [cf. *Lay and Bilek*, 2007], which may have aided in producing its remarkably large trans-Pacific tsunami. This hypothesized mechanism would result in a somewhat smaller M_w than used in the back-calculation of coseismic slip (M_t assumed to be equivalent to M_w) and, accordingly, lower average coseismic slip values. Globally, a 500–700 km long subduction megathrust rupture corresponds to an M_w of 8.9–9.1 and average coseismic slip of 8–12 m [*Papazachos et al.*, 2004]. Such values would better fit with the interseismic/coseismic budget of moment at the VS (Figure 17b).

For the much smaller 1737, 1742, and 1748 events, which may have involved only up to a few meters of coseismic slip, we suggest that they released only minor amounts of accumulated strain along the VS. Hence, their role in the accumulated moment budget of the seismic cycle seems to be of limited importance, which is in line with the inference that the 1960 event spent more or less the entire 385 years of interplate strain accumulation in the northern half of the VS (Figure 17). The combination of such a small 1737 event and the more southern (and trenchward?) 1837 event confirms the conclusion of *Cisternas et al.* [2005] that the 1960 event did not happen too early for its size, as was classically postulated [*Stein et al.*, 1986], but is a representative event of the seismic cycle in the Valdivia Segment.

In conclusion, these findings let us propose that the 1000 km long VS is subjected to a variable rupture mode in terms of rupture extent and coseismic slip. Three main groups of large earthquakes can be discerned:

1. Full ruptures, which took place in 1960, 1575, 1319 (±9), and 1127 (±44) and which can reach an M_w of 9.5 and slip values of 15–40 m.
2. Ruptures of the southern half of the VS like the one in 1837, with an M_w of ~9 and slip values of 8–15 m. Yet only one event of this kind at the VS has been identified in our records.
3. Smaller partial ruptures like the ones in 1737 and 1466 (±4) with an M_w of about 7¾ and coseismic slip values of a maximum of a few meters. These events do not seem to trigger devastating tsunamis.

Our lacustrine data confirm the average recurrence rate of 280 years for 1960-like earthquakes (M_w: 9.5) along the VS by *Cisternas et al.* [2005]. When lowering the magnitude threshold to $M_w \geq 7\,¾$, we find an average recurrence of 140 years for the latitude of Valdivia. Consequently, the seismic segmentation and variability in rupture mode—regardless of its physical cause—have important implications for estimating the short-to-midterm seismic hazard for this region. Yet more paleoseismic records of possibly complementary nature (among others lake records, marine records, tsunami records, etc.) are needed to constrain the exact rupture area of the 1737 and 1837 events and the paleo-earthquake parameters along the southern half of the VS.

7. Conclusions

This study came up with the following conclusions:

1. Lacustrine turbidites—in contrast to many other paleoseismic techniques—can form accurately dated and continuous paleoseismic records in settings with frequent occurrence of large earthquakes. All suitable sub-basins in glacigenic lakes Villarrica, Calafquén, and Riñihue in south central Chile contain a complete record of giant earthquakes ($I \geq$ VII½, $M_w \geq 9$) along the Valdivia Segment. Earthquakes at the adjacent Maule Segment did not significantly "contaminate" these lacustrine paleoseismic records as their imprint in the selected lakes is only minor with a distinct latitudinal gradient (i.e., 2010), or absent.
2. Small earthquakes with intensities as low as V½ can deposit a specific sedimentary trace at the foot of specific subaquatic slopes that are very susceptible for failure (e.g., delta fans). Hemipelagic lacustrine slopes in our study area only fail when seismic intensities exceed VI½.
3. The turbidites' thickness and spatial extent (i.e., volume of remobilized slope sediment) can reveal information about the seismic intensity (and thus also magnitude and/or rupture location) of paleo-earthquakes. A multibasin approach allows constructing multiscale paleoseismic records covering different seismic intensity thresholds.
4. The 2010 Maule earthquake may have produced stronger ground motions from its rupture zone toward the southeast, compared to previous megathrust events of similar size and location.
5. The 1837 earthquake may have played a significant role in releasing accumulated interseismic strain along the southern half of the VS. Its large trans-Pacific tsunami and interseismic/coseismic moment budget led us to suggest that it may have ruptured up to the trench region. In comparison, the 1737 was a minor event in terms of rupture extent, shaking strength, and coseismic slip.
6. Our lacustrine turbidite records confirm the presence and pinpoint the age of giant prehistorical earthquakes in 1319 (±9) and 1127 (±44), which were previously suggested by a coastal record of subsidence and tsunamis. Moreover, our records demonstrate the presence of a 1737-like partial rupture which took place around 1466 (±4).
7. Correlation of paleoseismic archives of the Valdivia Segment points to a variable rupture mode for the interplate surface in terms of rupture extent and coseismic slip during the last 900 years. This model includes three types of events: full 1960-like ruptures, "half" ruptures (e.g., 1837), and small partial ruptures (e.g., 1737). While M_w ~9.5 events take place about every 280 years at the VS [*Cisternas et al.*, 2005], the average recurrence rate including all $M_w \geq 7¾$ events at the latitude of Valdivia is about 140 years.

Acknowledgments
We acknowledge the financial support from the Swiss National Science Foundation (grant 133481), the Special Research funds of Ghent University (BOF), and the Research Foundation Flanders (FWO-Vlaanderen). M.V.D. thanks the GSA Limnogeology Division for the Kerry Kelts award and IAS for the postgraduate grant. K.F. is supported by NERC grant NE/I013210/1. IHS Kingdom is acknowledged for their educational grant program providing seismic interpretation software. We are grateful to Koen De Rycker, Robert Brümmer, Willem Vandoorne, and Alejandro Peña for technical support during fieldwork and Fabienne Masson for valuable artwork suggestions. Chris Goldfinger and an anonymous reviewer are acknowledged for their constructive reviews improving an earlier version of this paper.

References

Abe, K. (1979), Size of great earthquakes of 1837–1974 inferred from tsunami data, *J. Geophys. Res.*, *84*(B4), 1561–1568, doi:10.1029/JB084iB04p01561.

Angermann, D., J. Klotz, and C. Reigber (1999), Space-geodetic estimation of the Nazca-South America Euler vector, *Earth Planet. Sci. Lett.*, *171*, 329–334, doi:10.1016/S0012-821X(99)00173-9.

Arnaud, F., V. Lignier, M. Revel, M. Desmet, C. Beck, M. Pourchet, F. Charlet, A. Trentesaux, and N. Tribovillard (2002), Flood and earthquake disturbance of Pb-210 geochronology (Lake Anterne, NW Alps), *Terra Nova*, *14*(4), 225–232, doi:10.1046/j.1365-3121.2002.00413.x.

Astroza, M. I., M. H. Sandoval, and E. V. Kausel (2005), Estudio comparativo de los efectos de los sismos Chilenos de subducción del tipo intraplaca de profundidad intermedia, paper presented at Congreso Chileno de Sismología e Ingeniería Antisísmica, Concepción, Chile.

Avşar, U., A. Hubert-Ferrari, M. De Batist, and N. Fagel (2014), A 3400 year lacustrine paleoseismic record from the North Anatolian Fault, Turkey: Implications for bimodal recurrence behavior, *Geophys. Res. Lett.*, *41*, doi:10.1002/2013GL058221.

Barrientos, S. E. (1980), Regionalización sísmica de Chile, MS thesis, Univ. de Chile, Santiago, Chile.

Barrientos, S. E. (1988), Slip distribution of the 1985 central Chile earthquake, *Tectonophysics*, *145*(3–4), 225–241, doi:10.1016/0040-1951(88)90197-7.

Beck, C. (2009), Late Quaternary lacustrine paleo-seismic archives in north-western Alps: Examples of earthquake-origin assessment of sedimentary disturbances, *Earth Sci. Rev.*, *96*(4), 327–344, doi:10.1016/j.earscirev.2009.07.005.

Beck, S., S. Barrientos, E. Kausel, and M. Reyes (1998), Source characteristics of historic earthquakes along the central Chile subduction zone, *J. South Am. Earth Sci.*, *11*(2), 115–129, doi:10.1016/S0895-9811(98)00005-4.

Bertrand, S., F. Charlet, E. Chapron, N. Fagel, and M. De Batist (2008), Reconstruction of the Holocene seismotectonic activity of the Southern Andes from seismites recorded in Lago Icalma, Chile, 39°S, *Palaeogeogr. Palaeoclimatol. Palaeoecol.*, *259*(2–3), 301–322, doi:10.1016/j.palaeo.2007.10.013.

Blumberg, S., F. Lamy, H. W. Arz, H. P. Echtler, M. Wiedicke, G. H. Haug, and O. Oncken (2008), Turbiditic trench deposits at the South-Chilean active margin: A Pleistocene-Holocene record of climate and tectonics, *Earth Planet. Sci. Lett.*, *268*, 526–539, doi:10.1016/j.epsl.2008.02.007.

Boës, X., and N. Fagel (2008), Relationships between southern Chilean varved lake sediments, precipitation and ENSO for the last 600 years, *J. Paleolimnol.*, *39*, 237–252, doi:10.1007/s10933-007-9119-9.

Boroschek, R. L., V. Contreras, D. J. Kwak, and J. P. Stewart (2012), Strong ground motion attributes of the 2010 M_w 8.8 Maule, Chile, Earthquake. *Earthquake Spectra*, *28*(S1), 19–38, doi:10.1193/1.4000045.

Campos, H. (1984), Limnological study of Araucanian lakes (Chile), *Verh. Int. Ver. Limnol.*, *22*, 1319–1327.

Campos, H., W. Steffen, G. Agüero, O. Parra, and L. Zuñiga (1987), Limnology of lake Riñihue, *Limnologica*, *18*(2), 339–357.

Campos, J., D. Hatzfeld, R. Madariaga, G. Lopez, E. Kausel, A. Zollo, G. Iannacone, R. Fromm, S. Barrientos, and H. Lyon-Caen (2002), A seismological study of the 1835 seismic gap in south-central Chile, *Phys. Earth Planet. Inter.*, *132*, 177–195, doi:10.1016/S0031-9201(02)00051-1.

Chapron, E., C. Beck, M. Pourchet, and J. F. Deconinck (1999), 1822 earthquake-triggered homogenite in lake Le Bourget (NW Alps), *Terra Nova*, *11*(2–3), 86–92, doi:10.1046/j.1365-3121.1999.00230.x.

Chapron, E., D. Ariztegui, S. Mulsow, G. Villarosa, M. Pino, V. Outes, E. Juvignié, and E. Crivelli (2006), Impact of the 1960 major subduction earthquake in Northern Patagonia (Chile, Argentina), *Quat. Int.*, *158*, 58–71, doi:10.1016/j.quaint.2006.05.017.

Cifuentes, I. L. (1989), The 1960 Chilean earthquakes, *J. Geophys. Res.*, *94*(B1), 665–680, doi:10.1029/JB094iB01p00665.

Cisternas, M., et al. (2005), Predecessors of the giant 1960 Chile earthquake, *Nature*, *437*(7057), 404–407, doi:10.1038/nature03943.

Clare, M. A., P. J. Talling, P. Challenor, G. Malgesini, and J. Hunt (2014), Distal turbidites reveal a common distribution for large (>0.1 km^3) submarine landslide recurrence, *Geology*, doi:10.1130/G35160.1, in press.

Davis, S. N., and K. J. Karzulovic (1963), Landslides at Lago Rinihue, Chile, *Bull. Seismol. Soc. Am.*, *53*(6), 1403–1414.

DeMets, C., R. G. Gordon, and D. F. Argus (2010), Geologically current plate motions, *Geophys. J. Int.*, *181*(1), 1–80, doi:10.1111/j.1365-246X.2009.04491.x.

Fritz, H. M., et al. (2011), Field survey of the 27 February 2010 Chile tsunami, *Pure Appl. Geophys.*, *168*(11), 1989–2010, doi:10.1007/s00024-011-0283-5.

Geersen, J., D. Völker, J. H. Behrmann, D. Kläschen, W. Weinrebe, S. Krastel, and C. Reichert (2013), Seismic rupture during the 1960 Great Chile and the 2010 Maule earthquakes limited by a giant Pleistocene submarine slope failure, *Terra Nova*, *25*, 472–477, doi:10.1111/ter.12060.

Girardclos, S., O. T. Schmidt, M. Sturm, D. Ariztegui, A. Pugin, and F. S. Anselmetti (2007), The 1996 AD delta collapse and large turbidite in lake Brienz. *Mar. Geol.*, *241*(1–4), 137–154, doi:10.1016/j.margeo.2007.03.011.

Goldfinger, C. (2011), Submarine paleoseismology based on turbidite records, *Annu. Rev. Mar. Sci.*, *3*, 35–66.

Goldfinger, C., et al. (2012), Turbidite event history—Methods and implications for Holocene paleoseismicity of the Cascadia subduction zone, *U.S. Geol. Surv. Prof. Pap. 1661–F*, 170 p. [Available at http://pubs.usgs.gov/pp/pp1661f/.]

Goldfinger, C., Y. Ikeda, R. S. Yeats, and J. Ren (2013), Superquakes and supercycles, *Seismol. Res. Lett.*, *84*(1), doi:10.1785/0220110135.

Gràcia, E., A. Vizcaino, C. Escutia, A. Asioli, A. Rodés, R. Pallàs, J. Garcia-Orellana, S. Lebreiro, and C. Goldfinger (2010), Holocene earthquake record offshore Portugal (SW Iberia): Testing turbidite paleoseismology in a slow-convergence margin, *Quat. Sci. Rev.*, *29*(9–10), 1156–1172, doi:10.1016/j.quascirev.2010.01.010.

Hanks, T. C., and H. Kanamori (1979), A moment magnitude scale, *J. Geophys. Res.*, *84*(B5), 2348–2350, doi:10.1029/JB084iB05p02348.

Heezen, B. C., and M. Ewing (1952), Turbidity currents and submarine slumps, and the 1929 Grand Banks earthquake, *Am. J. Sci.*, *250*, 849–873, doi:10.2475/ajs.250.12.849.

Howarth, J. D., S. J. Fitzsimons, R. J. Norris, and G. E. Jacobsen (2012), Lake sediments record cycles of sediment flux driven by large earthquakes on the Alpine fault, New Zealand, *Geology*, *40*(12), 1091–1094, doi:10.1130/G33486.1.

Hubert-Ferrari, A., U. Avsar, M. El Ouahabi, G. Lepoint, P. Martinez, and N. Fagel (2012), Paleoseismic record obtained by coring a sag-pond along the North Anatolian Fault (Turkey), *Ann. Geophys.*, *55*(5), 929–953, doi:10.4401/ag-5460.

Inouchi, Y., Y. Kinugasa, F. Kumon, S. Nakano, S. Yasumatsu, and T. Shiki (1996), Turbidites as records of intense palaeoearthquakes in Lake Biwa, Japan, *Sediment. Geol.*, *104*(1–4), 117–125, doi:10.1016/0037-0738(95)00124-7.

Kanamori, H. (1983), Magnitude scales and quantification of earthquakes, *Tectonophysics*, *93*, 185–199, doi:10.1016/0040-1951(83)90273-1.

Karlin, R. E., and S. E. B. Abella (1992), Paleoearthquakes in the Puget Sound Region recorded in sediments from Lake Washington, U.S.A., *Science*, *258*(5088), 1617–1620, doi:10.1126/science.258.5088.1617.

Kelson, K., R. C. Witter, A. Tassara, I. Ryder, C. Ledezma, G. Montalva, D. Frost, N. Sitar, R. Moss, and L. Johnson (2012), Coseismic tectonic surface deformation during the 2010 Maule, Chile, *Mw* 8.8 earthquake, *Earthquake Spectra*, *28*(S1), 39–54, doi:10.1193/1.4000042.

Lange, D., J. Cembrano, A. Rietbrock, C. Haberland, T. Dahm, and K. Bataille (2008), First seismic record for intra-arc strike-slip tectonics along the Liquiñe-Ofqui fault zone at the obliquely convergent plate margin of the southern Andes, *Tectonophysics 455*, 14–24, doi:10.1016/j.tecto.2008.04.014.

Laugenie, C. (1982), La région des lacs, Chili méridional, PhD thesis, Université de Bordeaux III, Bordeaux, France.

Lay, T., and S. L. Bilek (2007), Anomalous earthquake ruptures at shallow depths on subduction zone megathrusts, in *The Seismogenic Zone of Subduction Thrust Faults*, edited by T. Dixon and C. Moore, pp. 476–511, Columbia Univ. Press, New York.

Lazo, R. G. H. (2008), Estudio de los daños de los terremotos del 21 y 22 de mayo de 1960, MSc thesis, Universidad de Chile, Santiago, Chile. [Available at http://www.tesis.uchile.cl/tesis/uchile/2008/lazo_rh/sources/lazo_rh.pdf.]

Leyton, F., S. Ruiz, and S. A. Sepúlveda (2010), Reevaluación del peligro sísmico probabilístico en Chile central, *Andean Geol.*, *37*(2), 455–472.

Lomnitz, C. (1970), Major earthquakes and tsunamis in Chile during the period 1535 to 1955, *Geol. Rundsch.*, *59*, 938–960, doi:10.1007/BF02042278.

Malgrange, M., A. Deschamps, and R. Madariaga (1981), Thrust and extensional faulting under the Chilean coast—1965, 1971 Aconcagua earthquakes, *Geophys. J. R. Astron. Soc.*, *66*(2), 313–331, doi:10.1111/j.1365-246X.1981.tb05958.x.

Masson, D. G., R. G. Arzola, R. B. Wynn, J. E. Hunt, and P. P. E. Weaver (2011), Seismic triggering of landslides and turbidity currents offshore Portugal, *Geochem. Geophys. Geosyst.*, *12*, Q120111, doi:10.1029/2011GC003839.

Melnick, D., B. Bookhagen, M. R. Strecker, and H. P. Echtler (2009), Segmentation of megathrust rupture zones from fore-arc deformation patterns over hundreds to millions of years, Arauco peninsula, Chile, *J. Geophys. Res.*, *114*, B01407, doi:10.1029/2008JB005788.

Melnick, D., M. Moreno, M. Cisternas, and A. Tassara (2012), Darwin seismic gap closed by the 2010 Maule earthquake, *Andean Geol. 39*(3), 558–563, doi:10.5027/andgeoV39n3-a11.

Meruane, C., Y. Niño, and R. Garreaud (2005), Response of the thermal structure of lake Villarrica (Chile) to strong foehn like wind: Field study and numerical simulations, MECOM, Universidad de Chile, Santiago, Chile. [Available at http://www.dgf.uchile.cl/rene/PUBS/Paper_Villarrica_borrador.pdf.]

Métois, M., A. Socquet, and C. Vigny (2012), Interseismic coupling, segmentation and mechanical behavior of the central Chile subduction zone, *J. Geophys. Res.*, *117*, B03406, doi:10.1029/2011JB008736.

Migowski, C., A. Agnon, R. Bookman, J. F. W. Negendank, and M. Stein (2004), Recurrence pattern of Holocene earthquakes along the Dead Sea transform revealed by varve-counting and radiocarbon dating of lacustrine sediments, *Earth Planet. Sci. Lett.*, *222*(1), 301–314, doi:10.1016/j.epsl.2004.02.015.

Moernaut, J. (2010), Sublacustrine landslide processes and their paleoseismological significance: Revealing the recurrence rate of giant earthquakes in south-central Chile, PhD thesis, Ghent University, Ghent, Belgium.

Moernaut, J., M. De Batist, F. Charlet, K. Heirman, E. Chapron, M. Pino, R. Brummer, and R. Urrutia (2007), Giant earthquakes in south-central Chile revealed by Holocene mass-wasting events in Lake Puyehue, *Sediment. Geol.*, *195*(3–4), 239–256, doi:10.1016/j.sedgeo.2006.08.005.

Moernaut, J., M. De Batist, K. Heirman, M. Van Daele, M. Pino, R. Brümmer, and R. Urrutia (2009), Fluidization of buried mass-wasting deposits in lake sediments and its relevance for paleoseismology: Results from a reflection seismic study of lakes Villarrica and Calafquén (south-central Chile), *Sediment. Geol.*, *213*, 121–135, doi:10.1016/j.sedgeo.2008.12.002.

Monecke, K., F. S. Anselmetti, A. Becker, M. Sturm, and D. Giardini (2004), The record of historic earthquakes in lake sediments of Central Switzerland, *Tectonophysics*, *394*(1–2), 21–40, doi:10.1016/j.tecto.2004.07.053.

Moreno, M. S., J. Bolte, J. Klotz, and D. Melnick (2009), Impact of megathrust geometry on inversion of coseismic slip from geodetic data: Application to the 1960 Chile earthquake, *Geophys. Res. Lett.*, *36*, L16310, doi:10.1029/2009GL039276.

Moreno, M., et al. (2011), Heterogeneous plate locking in the south-central Chile subduction zone: Building up the next great earthquake, *Earth Planet. Sci. Lett.*, *305*(3–4), 413–424, doi:10.1016/j.epsl.2011.03.025.

Moreno, M., et al. (2012), Toward understanding tectonic control on the *Mw* 8.8 2010 Maule Chile earthquake, *Earth Planet. Sci. Lett.*, *321–322*, 152–165, doi:10.1016/j.epsl.2012.01.006.

Musson, R. M. W., G. Gruenthal, and M. Stucchi (2010), The comparison of macroseismic intensity scales, *J. Seismol.*, *14*, 413–428, doi:10.1007/s10950-009-9172-0.

Nishenko, S. P. (1985), Seismic potential for large and great interplate earthquakes along the Chilean and Southern Peruvian margins of South America: A quantitative reappraisal. *J. Geophys. Res.*, *90*, 3589–3615, doi:10.1029/JB090iB05p03589.

Papazachos, B. C., E. M. Scordilis, D. G. Panagiotopoulos, C. B. Papazachos, and G. F. Karakaisis (2004), Global relations between seismic fault parameters and moment magnitude of earthquakes, *Bull. Geol. Soc. Greece*, *36*, 1482–1489.

Polonia, A., G. Panieri, L. Gasperini, G. Gasparotto, L. G. Bellucci, and L. Torelli (2013), Turbidite paleoseismology in the Calabrian Arc Subduction Complex (Ionian Sea), *Geochem. Geophys. Geosyst.*, *14*, 112–140, doi:10.1029/2012GC004402.

Pouderoux, H., G. Lamarche, and J.-N. Proust (2012), Building an 18 000-year-long paleo-earthquake record from detailed deep-sea turbidite characterisation in Poverty Bay, New Zealand, *Nat. Hazards Earth Syst. Sci.*, *12*, 2077–2101, doi:10.5194/nhess-12-2077-2012.

Pouderoux, H., J.-N. Proust, and G. Lamarche (2014), Submarine paleoseismology of the northern Hikurangi subduction margin of New Zealand as deduced from turbidite record since 16 ka, *Quat. Sci. Rev.*, *84*, 116–131, doi:10.1016/j.quascirev.2013.11.015.

Rosenau, M., D. Melnick, and H. Echtler (2006), Kinematic constraints on intra-arc shear and strain partitioning in the southern Andes between 38°S and 42°S latitude, *Tectonics*, *24*, TC4013, doi:10.1029/2005TC001943.

Saragoni, G. R., M. Astroza, and S. Ruiz (2004), Comparative study of subduction earthquake ground motion of North, Central and South America, paper presented at 13th World Conference on Earthquake Engineering, Vancouver B.C., Canada.

Satake, K., and B. F. Atwater (2007), Long-term perspectives on giant earthquakes and tsunamis at subduction zones, *Ann. Rev. Earth Planet. Sci.*, *35*, 349–274, doi:10.1146/annurev.earth.35.031306.140302.

Schnellmann, M., F. S. Anselmetti, D. Giardini, J. A. McKenzie, and S. N. Ward (2002), Prehistoric earthquake history revealed by lacustrine slump deposits, *Geology*, *30*, 1131–1134, doi:10.1130/0091-7613.

SHOA (Servicio Hidrográfico y Oceanográfico de la Armada de Chile) (1987), Lago Villarrica, scale 1:40,000, Santiago, Chile.

SHOA (Servicio Hidrográfico y Oceanográfico de la Armada de Chile) (2008), Lago Calafquén, scale 1:30,000, Santiago, Chile.

Sievers, H. (2000), El maremoto del 22 mayo de 1960 en las costas de Chile. Servicio Hidrográfico y Oceanográfico de la Armada de Chile, 2a Edición, Santiago, Chile.

Silva Parejas, C., T. H. Druitt, C. Robin, H. Moreno, and J.-A. Naranjo (2010), The Holocene Pucón eruption of Volcán Villarrica, Chile: Deposit architecture and eruption chronology, *Bull. Volcanol.*, *72*, 677–692, doi:10.1007/s00445-010-0348-9.

Sims, J. D. (1973), Earthquake-induced structures in sediments of Van Norman Lake, San Fernando, California, *Science*, *182*(4108), 161–163, doi:10.1126/science.182.4108.161.

SISRA (1985), Datos de Hipocentros y Intensidades en Chile, in *Catalogo de Terremotos para America del Sur (CERESIS)*, vol. 5, edited by T. Algermissen and B. Askew, pp. 4–96, CERESIS, Lima, Peru.

Smith, S. B., R. E. Karlin, G. M. Kent, G. G. Seitz, and N. W. Driscoll (2013), Holocene subaqueous paleoseismology of Lake Tahoe. *Geol. Soc. Am. Bull.*, *125*(5–6), 691–708, doi:10.1130/B30629.1.

Sparkes, R., F. Tilmann, N. Hovius, and J. Hillier (2010), Subducted seafloor relief stops rupture in South American great earthquakes: Implications for rupture behaviour in the 2010 Maule, Chile earthquake, *Earth Planet. Sci. Lett.*, *298*(1–2), 89–94, doi:10.1016/j.epsl.2010.07.029.

Stein, S., J. F. Engeln, C. DeMets, R. G. Gordon, D. Woods, P. Lundgren, D. Argus, C. Stein, and D. A. Wiens (1986), The Nazca-South American convergence rate and the recurrence of the great 1960 Chilean earthquake. *Geophys. Res. Lett.*, *13*(8), 713–716, doi:10.1029/GL013i008p00713.

St-Onge, G., et al. (2012), Comparison of earthquake-triggered turbidites from the Saguenay (Eastern Canada) and Reloncavi (Chilean margin) Fjords: Implications for paleoseismicity and sedimentology, *Sediment. Geol.*, *243*, 89–107, doi:10.1016/j.sedgeo.2011.11.003.

Strasser, M., F. S. Anselmetti, D. Fah, D. Giardini, and M. Schnellmann (2006), Magnitudes and source areas of large prehistoric northern Alpine earthquakes revealed by slope failures in lakes, *Geology*, *34*(12), 1005–1008, doi:10.1130/G22784A.1.

Strasser, M., M. Hilbe, and F. S. Anselmetti (2011), Mapping basin-wide subaquatic slope failure susceptibility as a tool to assess regional seismic and tsunami hazards, *Mar. Geophys. Res.*, *32*(1–2), 331–347, doi:10.1007/s11001-010-9100-2.

Tassara, A., H. J. Gotze, S. Schmidt, and R. Hackney (2006), Three-dimensional density model of the Nazca plate and the Andean continental margin, *J. Geophys. Res.*, *111*, B09404, doi:10.1029/2005JB003976.

Ten Brink, U. S., H. J. Lee, E. L. Geist, and D. Twichell (2009), Assessment of tsunami hazard to the U.S. East Coast using relationships between submarine landslides and earthquakes, *Mar. Geol.*, *264*, 65–73, doi:10.1016/j.margeo.2008.05.011.

U.S. Geological Survey (2010), USGS Community Internet Intensity Map (Offshore Maule, Chile). [Available at http://earthquake.usgs.gov/earthquakes/dyfi/events/us/2010tfan/us/index.html.]

U.S. Geological Survey (2011), USGS Community Internet Intensity Map (M7.1 - Araucania, Chile). [Available at http://earthquake.usgs.gov/earthquakes/dyfi/events/us/c0000y49/us/index.html.]

Udías, A., R. Madariaga, E. Buforn, D. Muñoz, and M. Ros (2012), The large Chilean historical earthquakes of 1647, 1657, 1730 and 1751 from contemporary documents. *Bull. Seismol. Soc. Am.*, *102*(4), 1639–1653, doi:10.1785/0120110289.

Van Daele, M., W. Versteeg, M. Pino, R. Urrutia, and M. De Batist (2013), Widespread deformation of basin-plain sediments in Aysén fjord (Chile) due to impact by earthquake-triggered, onshore-generated mass movements, *Mar. Geol.*, *337*, 67–79, doi:10.1016/j.margeo.2013.01.006.

Van Daele, M., et al. (2014), The 600 year eruptive history of Villarrica Volcano (Chile) revealed by annually-laminated lake sediments, *Geol. Soc. Am. Bull.*, doi:10.1130/B30798.1, in press.

Völker, D., I. Grevemeyer, M. Stipp, K. Wang, and J. He (2011), Thermal control of the seismogenic zone of southern central Chile, *J. Geophys. Res.*, *116*, B10305, doi:10.1029/2011JB008247.

Waldmann, N., F. S. Anselmetti, D. Ariztegui, J. A. Austin, M. Pirouz, C. M. Moy, and R. Dunbar (2011), Holocene mass-wasting events in Lago Fagnano, Tierro del Fuego (54°S): Implications for paleoseismicity of the Magallanes-Fagnano transform fault, *Basin Res.*, *23*, 171–190, doi:10.1111/j.1365-2177.2010.00489.x.

Wang, K., Y. Hu, M. Bevis, E. Kendrick, R. Smalley, R. B. Vargas, and E. Lauria (2007), Crustal motion in the zone of the 1960 Chile earthquake: Detangling earthquake-cycle deformation and forearc-sliver translation, *Geochem. Geophys. Geosyst.*, *8*, Q10010, doi:10.1029/2007GC001721.

Zobin, V. M. (2001), Seismic hazard of volcanic activity, *J. Volcanol. Geotherm. Res. 112*, 1–14, doi:10.1016/S0377-0273(01)00230-X.